Decoupling of $\Delta O_2/Ar$ and particulate organic carbon dynamics in near shore surface ocean waters

Sarah Z. Rosengard[1], Robert W. Izett[1], William J. Burt[2], Nina Schuback[3], and Philippe D. Tortell[1,4]

1. Department of Earth, Ocean and Atmospheric Sciences, University of British Columbia, Vancouver, V6T 1Z4, Canada
2. College of Fisheries and Ocean Sciences, University of Alaska Fairbanks, Fairbanks, 99775, USA
3. Institute of Geological Sciences and Oeschger Center for Climate Change Research, University of Bern, Bern, Switzerland
4. Department of Botany, University of British Columbia, Vancouver, V6T 1Z4, Canada

Correspondence to: Sarah Z. Rosengard (srosengard@eoas.ubc.ca)

Abstract. We report results from two Lagrangian drifter surveys off the Oregon coast, using continuous ship-board sensors to estimate mixed layer gross primary productivity (GPP), community respiration (CR), and net community production (NCP) from variations in biological oxygen saturation ($\Delta O_2/Ar$) and optically-derived particulate organic carbon (POC). At the first drifter survey, conducted in a nearshore upwelling zone during the development of a microplankton bloom, net changes in $\Delta O_2/Ar$ and [POC] were significantly decoupled. Differences in GPP and NCP derived from $\Delta O_2/Ar$ ($NCP_{O2/Ar}$) and POC (NCP_{POC}) time series suggest the presence of large POC losses from the mixed layer. At this site, we utilized the discrepancy between $NCP_{O2/Ar}$ and NCP_{POC}, and additional constraints derived from surface water excess nitrous oxide (N_2O), to evaluate POC loss through particle export, DOC production and vertical mixing fluxes. At the second drifter survey, conducted in lower productivity, density-stratified offshore waters, we also observed offsets between $\Delta O_2/Ar$ and POC-derived GPP and CR rates. At this site, however, net [POC] and $\Delta O_2/Ar$ changes yielded closer agreement in NCP estimates, suggesting a tighter relationship between production and community respiration, and lower POC loss rates. These results provide insight into the possibilities and limitations of estimating productivity from continuous underway POC and $\Delta O_2/Ar$ data in contrasting oceanic waters. Our observations support the use of diel POC measurements to estimate NCP in lower productivity waters with limited vertical carbon export, and the potential utility of coupled O_2 and optical measurements to estimate the fate of POC in high productivity regions with significant POC export.

1 Introduction

Marine primary productivity provides the main source of organic carbon to the ocean, supporting the vast majority of marine ecosystem biomass. On short time scales, a large fraction of this fixed organic carbon is converted back to CO_2 through community respiration (CR). The difference between gross primary productivity (GPP) and CR – net community production (NCP) – sets an upper limit on the quantity of particulate organic carbon that can be exported out of the mixed layer as sinking particles, transferred to the dissolved organic carbon (DOC) pool, or consumed by upper trophic levels. Accurate assessment of NCP is thus critical to understanding trophic balance and the fate of organic carbon in the surface ocean. Traditional

47 incubation-based approaches to quantify GPP, net primary productivity (NPP) and CR are labor-

48 intensive and prone to sample containment artifacts (Gieskes et al., 1979; Fogg and Calvario-

49 Martinez, 1989; Marra, 2009; Quay et al., 2010), such that NCP remains challenging to quantify

50 on ecologically-relevant time and space scales.

51   In recent years, automated *in situ* measurements of seawater optical properties have been

52 increasingly used to estimate gross and net primary productivity from changes in optically-

53 derived surface water POC concentrations (e.g., Graff et al., 2016; Burt et al., 2018). This

54 approach is based on the relationship between POC concentrations and the particulate fraction of

55 the beam attenuation coefficient (c_p) (Siegel et al., 1989; Stramska and Dickey, 1992; Gardner et

56 al., 1993; Claustre et al., 1999; Gernez et al., 2011), which can be used to resolve diurnal

57 variations in POC. This diurnal variability results from the daytime accumulation of

58 photosynthetically-produced organic carbon, and nighttime loss of fixed carbon through

59 community respiration, and can thus be used to infer NCP on daily time-scales. The accuracy of

60 this approach depends on the key assumption that variations in c_P capture most of the variability

61 in POC concentration, and it has been shown that beam attenuation is most sensitive to particles

62 with a diameter range of 0.5–20 µm (Stramski and Kiefer 1991; Marra, 2002; Claustre et al.,

63 2008). To date, most efforts to calculate daily NCP from c_P variability have focused on low

64 productivity offshore regions, where particle sizes are small and POC losses through particle

65 export are limited (Claustre et al., 2008; White et al., 2017). These studies have reported good

66 agreement between optically-derived GPP estimates and independent estimates of NPP from 14C

67 incubations (White et al., 2017), suggesting a tight coupling between primary productivity and

68 mixed layer POC dynamics over daily time scales.

69   Another approach to NCP quantification is based on autonomous measurements of

70 surface water dissolved oxygen to argon ratios (O_2/Ar). Argon normalization is used to correct

71 for any physically-induced changes in O_2 saturation, such that the derived saturation anomaly,

72 ΔO_2/Ar, is a tracer of net biological O_2 production (Kaiser et al., 2005; Tortell, 2005; Cassar et

73 al., 2009). At steady-state, and in the absence of significant lateral advection and vertical mixing,

74 the sea-air flux of excess biologically-produced O_2 is equivalent to NCP. With the development

75 of automated ship-board mass spectrometers, there has been a significant expansion of surface

76 water O_2/Ar measurements. These data have been used to examine O_2 variability resulting from

77 diurnal variations of photosynthesis and respiration, and to infer NCP in a variety of oceanic

78 ecosystems (Reuer et al., 2007; Stanley et al., 2010; Tortell et al., 2011, 2014; Hamme et al.,

79 2012; Nicholson et al., 2015; Manning et al., 2017). Recent efforts have shown that NCP

80 estimates from $\Delta O_2/Ar$ measurements can be corrected for vertical mixing using water column

81 N_2O measurements as a tracer (Cassar et al. 2014; Izett et al. 2018), but application of this

82 methodology assumes that lateral advective fluxes of O_2 are negligible.

83   Combined measurement of mixed layer POC and O_2 dynamics holds the potential to

84 better constrain surface water carbon budgets in biogeochemically dynamic regions at high

85 spatial and temporal resolution. In net autotrophic systems, an increase in $\Delta O_2/Ar$ reflects the

86 accumulation of excess photosynthetic O_2 in the mixed layer, but provides no direct insight into

87 the fate of the resulting organic carbon. In the absence of particle export, grazing or DOC

88 production, an increase in $\Delta O_2/Ar$, corrected for air-sea exchange and vertical mixing, should be

89 matched by a parallel increase in POC accumulation measured by optical sensors. By

90 comparison, high POC export, DOC production or grazing coupled to vertical migrations would

91 act to decouple $\Delta O_2/Ar$ from optically-derived POC measurements in the mixed layer.

92   Previous authors have used simultaneous O_2 and c_p measurements on moorings to

93 describe mixed layer O_2 and POC dynamics in various marine environments (Stramska and

94 Dickey, 1992; Kinkade et al., 1999; Dickey and Chang, 2002). However, few studies to date

95 have compared estimates of primary productivity from simultaneous measurements on daily time

96 scales. Briggs et al. (2018) and Alkire et al. (2012) were the first to explicitly combine

97 concurrent measurements of O_2 and POC from *in situ* autonomous sensors to quantify mixed

98 layer productivity during a ~2-month Lagrangian study of the 2008 North Atlantic spring bloom.

99 Tracking daily changes in mixed layer O_2 and POC concentrations, Alkire et al. (2012)

100 constructed a detailed budget of surface ocean organic carbon throughout the course of the

101 bloom, using the difference between O_2-based NCP and net POC accumulation to assess the

102 partitioning of NCP into different carbon pools (sinking particles, phytoplankton biomass, and

103 DOC). Building on this work, Briggs et al. (2018) examined the role of respiration, particle

104 export, and DOC production in decoupling O_2 and POC dynamics through different bloom

105 stages, demonstrating significant differences between GPP estimates derived from O_2, beam

106 attenuation, and backscatter measurements. To our knowledge, such a detailed examination of O_2

107 and POC dynamics has not been reported for other marine systems.

108   Here, we present new results from a field study of diel variability in $\Delta O_2/Ar$ and optical

109   properties in two contrasting near-shore regions of the Subarctic North Pacific. Using ship-board

110   automated sensors deployed along a Lagrangian drifter track, we resolved fine-scale temporal

111   patterns in biological oxygen production and POC concentration in a high productivity coastal

112   upwelling zone over the continental slope and in lower productivity stratified waters offshore.

113   The biogeochemical differences between both sites provided a unique opportunity to compare

114   GPP, CR and NCP estimates derived from $\Delta O_2/Ar$ and POC in contrasting trophic regimes. We

115   expected to observe significant differences between $\Delta O_2/Ar$ and POC-derived GPP, CR, and

116   NCP estimates in the higher productivity site, reflecting greater carbon export capacity and DOC

117   production. By comparison, we hypothesized that discrepancies in these rates would be smaller

118   at the lower productivity site, reflecting a tighter coupling between O_2 and POC dynamics.

119   The results of this investigation extend the results from the 2008 North Atlantic bloom to

120   a high productivity coastal upwelling environment where vertical mixing fluxes significantly

121   influence the surface water mass balance. These dynamic systems play a disproportionately

122   important role in marine biogeochemical cycling, but they pose significant challenges for

123   interpreting time series of ecosystem metabolism. Furthermore, our study results further expand

124   applications of a recent field approach to correcting NCP for vertical mixing (Izett et al., 2018),

125   suggesting that this approach has significant merit in reconstructing productivity estimates from

126   a variety of mixed layer tracers. We discuss the implications of our coupled O_2-POC

127   measurements for understanding biological carbon cycling in marine waters, and suggest some

128   approaches to improve the utility of these measurements for evaluating the fate of marine

129   primary productivity across marine trophic gradients.

130

131   **2 Methods**

132

133   **2.1 Field site and Lagrangian surveys**

134

135   Field studies were conducted on board the R/V *Oceanus* in August 2017, during a

136   transect through the Northeast Subarctic Pacific Ocean. Two Lagrangian drifters were deployed

137   off the Oregon coast, allowing us to track diurnal patterns in phytoplankton productivity and

138   particulate organic carbon cycling in two distinct water masses (Fig. 1). Underway temperature

139   and salinity measurements, collected by a Seabird SBE 45 thermosalinograph, as well as satellite

140   (Aqua MODIS) and ship-based chlorophyll-a (Chl-a) observations, were used to guide the

141   specific location and timing of the drifter deployments. Drifter 1 was deployed on 20 August

142   2017 (~9:30 PDT), ~40 km from the Oregon coast (44.54° N, 124.58° W), in the vicinity of an

143   upwelling feature detected based on low sea surface temperature, and elevated salinity and [Chl-

144   a]. The drifter, consisting of a beacon, GPS transmitter and 5 m drogue, was recovered at ~18:30

145   on 23 August 2017 (44.40° N, 124.55° W) for a total deployment of 3 days and 9 hours. Upon

146   recovery, the drogue was missing, implying the potential for some erratic sub-surface drifting

147   (discussed below). Drifter 2 was deployed approximately 200 km from shore (43.75° N, 126.50

148   °W) in a relatively warm and low salinity water mass, with low Chl-a concentrations. This

149   second drifter was deployed at ~07:45 on 24 August 2017, and was recovered after 2 days and

150   six hours at ~14:00 on 26 August 2017 at 43.80° N, 126.99° W. Because the *Oceanus* lacks a

151   dynamic positioning system, the ship was not always able to perfectly track the drifter locations.

152   To correct for these positional offsets, we discarded any observations obtained when the ship

153   was more than 1.5 km away from the drifter location. This filtered dataset resulted in underway

154   measurements (Sect. 2.2) every ~15 minutes during the two drifter deployments, yielding 325

155   and 218 quality-controlled underway observations for drifters 1 and 2, respectively.

156

157   **2.2 Underway measurements**

158

159   Continuous underway measurements of surface seawater optical properties were

160   collected using Seabird (formerly Wetlabs) ECO-BB3 and ac-s sensors, following the methods

161   outlined in detail by Burt et al. (2018). Water was collected from the ship's seawater supply

162   system with a nominal intake of 5 m depth. Our instrument package included fully automated

163   data collection, and hourly filtered blanks (0.2µm), which provided measurements of dissolved

164   seawater optical properties used to infer particulate absorption (a_p) and beam attenuation (c_p) at

165   82 wavelengths between 400 and ~735 nm, and backscatter (b_{bp}) at 470 nm, 532 nm, and 650

166   nm. The BB-3 and ac-s measurements were binned into 1-minute intervals. Prior to binning, the

167   absorption and beam attenuation data were first sub-sampled every 50 data acquisition cycles

168   (~12.5 seconds) to enable faster processing time. The optical measurements were accompanied

169   by continuous surface photosynthetically active radiation (PAR) and windspeed data obtained

170   from a Biospherical QSR-220 PAR sensor and Gill WindObserver II ultrasonic wind sensor

171   mounted on the ship's bow.

172   Chlorophyll-a (Chl-a) concentrations were derived from the particulate absorption line

173   height at 676 nm (a_{LH}) (Roesler and Barnard, 2013). Five-minute match-ups between underway

174   a_{LH} and discrete filtered [Chl-a] measurements from the entire cruise transect (Sect. 2.4) were

175   used to derive a best fit coefficient for the linear relationship between a_{LH} and [Chl-a] (r_2=0.87,

176   n= 58, p<0.01). Particulate organic carbon (POC) concentrations (µg/L) were derived from

177   particulate beam attenuation at 660 nm ($c_{p,660}$), using the empirical model in Graff et al. (2015).

178   Similarly, phytoplankton organic carbon (C_{ph}) concentrations were calculated, using an empirical

179   relationship between particulate backscatter at 470 nm ($b_{bp,470}$) and [C_{ph}] in µg/L (Graff et al.,

180   2015). We used a limited set of 5m discrete measurements (n=6; Sect. 2.4) to evaluate the

181   relationship between POC concentrations and c_p at 660nm, and the applicability of the Graff et

182   al. (2015) model to our observations. As shown in Fig. S1, the POC measurements were

183   significantly correlated to c_p (r_2=0.88, p<0.05), with a slope and intercept of 391.6 $\pm$ 201.6 and

184   36.7 $\pm$ 79.1, respectively. This slope was not significantly different from that of the Graff et al.

185   algorithm (419.8) although our y-intercept was higher. Notwithstanding the relatively small

186   number of discrete POC samples, and some scatter around the regression line, the similarity of

187   our POC-c_p calibration to that reported by Graff et al. (2015) suggests that our optically-derived

188   POC estimates are reasonably robust.

189   To obtain information on the particle size spectrum, we derived the wavelength-

190   dependent slope of particulate backscatter by fitting the three b_{bp} coefficients (470 nm, 532 nm,

191   650 nm) to an exponential equation (Stramska et al., 2003; Loisel et al., 2006; Kostadinov et al.,

192   2009). Finally, to assess interference of inorganic minerals on POC, and C_{ph} variability, we

193   calculated the wavelength-specific bulk refractive index (η_p) from backscatter/total scatter ratios

194   ($\frac{b_{bp}}{c_p - a_p}$) and the wavelength-dependent c_p slope, following the approach of Boss et al. (2001),

195   Twardowski et al. (2001) and Sullivan et al. (2005).

196   In addition to optical measurements, the seawater biological oxygen saturation anomaly

197   ($\Delta O_2/Ar$) was measured at a ~20 second resolution using a membrane inlet mass spectrometer

198   connected to the ship's seawater intake. The seawater ratio of dissolved O_2 and Ar was

199   determined by diverting a continuous flow of water across a dimethylsilicone membrane

200   interfaced with a Hiden Analytical HAL20 triple filter quadropole mass spectrometer. The O_2/Ar

201 ratio of air-equilibrated standards ($[O_2/Ar]_{eq}$), incubated at ambient sea surface temperature, was

202 measured every two hours. Values of $\Delta O_2/Ar$ were thus calculated as the percent deviation of

203 seawater O_2/Ar measurements from the air-equilibrated ratio, using $\Delta O_2/Ar = 100\%$ *

204 ($[O2/Ar]_{meas} / [O2/Ar]_{eq} - 1$) (Tortell, 2005; Tortell et al., 2011).

205

206 **2.3 Mixed layer depth**

207

208   Over the course of both drifter deployments, we conducted regular sampling casts (every

209 six to ten hours) to examine depth profiles of seawater hydrography and biogeochemical

210 variables. Temperature, salinity, dissolved O_2 concentrations and Chl-a fluorescence profile data

211 from the CTD casts were measured by a Seabird-SBE 38 temperature sensor, Seabird-SBE 4

212 conductivity sensor, SBE 43 dissolved O_2 sensor, and a Seabird ECO fluorometer, respectively,

213 and binned into 1 m intervals. Vertical profiles at the drifter 1 site showed relatively weak

214 density stratification, likely as a result of recent upwelling. For this reason, we estimated mixed

215 layer depths (z_{mld}) based on visible inflection points in the dissolved $[O_2]$, fluorescence and

216 density profiles, assuming that dissolved O_2 concentrations and fluorescence are relatively

217 uniform in the mixed layer. Within a single CTD cast, mixed layer depths varied by up to 28%

218 across all three profile measurements. The [Chl-a] fluorescence profiles had the most well-

219 defined inflection points, and we thus used these data to estimate z_{mld} at all casts. Excluding

220 fluorescence profiles from the first day (Sect. 3.1), and two casts at 6am and midnight on second

221 and third 24-hour intervals, respectively, which displayed relatively noisy density profiles, an

222 average z_{mld} value (19 ± 2 m) was derived and applied to all subsequent analyses.

223   In comparison to the drifter 1 site, CTD cast profiles during drifter deployment 2 showed

224 larger density gradients. We thus computed z_{mld} using a density difference criterion of 0.25

225 kg/m3 (Thomson et al., 2003; de Boyer Montégut et al., 2004) from median values within the

226 upper-most 4–6 m of the profile. We found that this critical density criterion was necessary to

227 capture the depth of inflection in O_2 and [Chl-a]. In all CTD casts except one, density difference-

228 based z_{mld} values were within 5 meters of the values derived from the inflection points on density

229 profiles. An average z_{mld} value estimated from the density-difference approach (22 ± 5 m) was

230 applied to all subsequent analyses.

231

2.4 Discrete samples

Concentrations of phosphate ($[PO_4^{3-}]$), dissolved silica ($[SiO_2]$), and nitrate and nitrite ($[NO_3^- + NO_2^-]$, were measured in seawater samples collected from daily Niskin bottle casts. Following collection, nutrient samples were filtered through 0.2 µm pore polycarbonate membranes and immediately frozen at -80°C on board the ship. These samples were stored at -20°C until subsequent colorimetric laboratory analyses (Murphy and Riley, 1962; Riley, 1977) with a Lachat QuikChem 8500 Series 2 Flow Injection Analysis System.

Concentrations of nitrous oxide (N_2O) were measured in discrete samples collected in Niskin bottles during both drifter deployments (Fig. S2), following methods outlined in (Capelle et al., 2015). These N_2O measurements were used to correct NCP estimates for vertical mixing (see Sect. 2.6), following the approach described by Cassar et al. (2014) and Izett et al. (2018). Profile samples from the first day of drifter deployment 1 (August 20) were omitted from calculations, as underway surface temperature and salinity measurements indicated intrusion of an external water mass (further discussed in Sect. 3.1) (Fig. S3). Three profiles collected from 12:00 (PDT) CTD casts during the following three days of the deployment (August 21, 22 and 23) were applied to the NCP mixing correction at drifter station 1 (Sect. 2.6.1).

Surface (~5 m) discrete seawater samples were collected either from Niskin bottles or from the ship's surface seawater intake system for HPLC analysis of Chl-a concentrations and other phytoplankton pigments. Single or duplicate samples were filtered onto 25 mm GF/F filters, flash-frozen in liquid nitrogen, and stored at -80°C until analysis, following the methodology described in Schuback et al. (2016). Additional samples were collected from the seawater intake for size-fractionated Chl-a analysis (Zeng et al., 2018). These samples were filtered through stacked 47 mm filters (0.2 µm, 2 µm and 20 µm pore size) separated by a mesh spacer. Filtered samples were extracted in 5 mL of 90% acetone at 4°C until analysis within 24–48 hours using a Turner Trilogy Fluorometer on board the ship.

Discrete samples for POC analysis were collected at two depths from several CTD casts. Surface samples were collected at both drifter sites from 5 m depth, while deeper samples were collected at near the base of the euphotic zone (~1% PAR), corresponding to 40–60 m at drifter site 1, and 100–120 m at drifter site 2. POC samples (~1–4 L) were filtered through a pre-combusted (450 °C) Whatman GF/F filter (nominal pore size ~ 0.7 µm), and stored at -80°C

263   until laboratory analysis. Prior to analysis, samples were thawed and dried at 50°C overnight,

264   fumigated with concentrated hydrochloric acid for 48 hours, and dried again at 50°C overnight.

265   POC concentrations in samples (and blank combusted filters treated as described above) were

266   quantified using an *Elementar* vario MICRO cube CHNS analyzer. Blank-corrected discrete

267   POC concentrations were used to validate application of the [POC] model in Graff et al. (2015)

268   to our underway c_p data (Sect. 2.2; Fig. S1).

269

270   **2.5 Net Primary Productivity**

271

272   Daily-integrated net primary productivity (NPP) was calculated in two ways. First,

273   carbon uptake was determined from 24-hour $14C$-incubations with 5 m triplicate seawater

274   samples collected from early morning CTD casts. Measurements were made on two different

275   mornings during drifter deployment 1 and on one morning during drifter deployment 2. The

276   measurements were conducted following the protocol outlined in Hoppe et al. (2017). Depth-

277   integrated NPP was calculated by multiplying the derived 24-hour volumetric carbon fixation

278   rate by the average mixed layer depth for the respective drifter period.

279   Second, daily-integrated net primary productivity was also estimated as a product of $[C_{ph}]$

280   values derived from b_{bp}, and phytoplankton growth rates according to the carbon-based

281   production model (CbPM) (Behrenfeld et al., 2005; Westberry et al., 2008; Graff et al., 2016;

282   Burt et al., 2018). In these calculations, daily-averaged $[C_{ph}]$, $[Chl-a]/[C_{ph}]$, and mixed layer

283   irradiance (E_g) calculated from the MODIS-derived surface PAR matched to drifter location

284   were used to calculate growth rates and NPP every 24 hours. Chlorophyll-a concentrations were

285   derived from absorption line height, $[C_{ph}]$ values from b_{bp} (Sect. 2.2), and light extinction

286   coefficients (K_d) obtained from [Chl-a] to calculate E_g (Morel et al., 2007). An average mixed

287   layer depth for each drifter period was applied to estimate mixed layer NPP (Sect. 2.3).

288

289   **2.6 Quantification of GPP, CR and NCP**

290

291   Gross primary productivity (GPP), community respiration (CR) and net community

292   production (NCP) rates were calculated based on linear regressions of $\Delta O_2/Ar$ and POC against

293   time (dt in units of days) over subsequent day (D) and night (N) intervals during both drifter

294   deployments. Daytime was defined as the period during which PAR levels exceeded 20 µ mol

295   quanta m$_{-2S-1}$. The average length of the day-time period was 13.6 ± 0.14 hours over the two

296   drifter deployments. In the following sections, t_d represents the day length normalized to 24

297   hours, and t_n analogously represents the fractional night length, equivalent to $1-t_d$. All daily rates

298   were integrated through the mixed layer using the average z_{mld} for each drifter period, as

299   described in Sect. 2.3.

300

301   **2.6.1 O$_2$/Ar-derived rates**

302

303   Quantification of GPP$_{O2/Ar}$, CR$_{O2/Ar}$, and NCP$_{O2/Ar}$ rates from diurnal cycles in ΔO_2/Ar

304   (Ferrón et al., 2015) requires corrections for gas exchange and, potentially, vertical mixing

305   fluxes. For these calculations, we first computed the rate of change in ΔO_2/Ar (dO$_{2Bio}$/dt) using

306   linear regression analysis within successive day or night intervals. We then derived estimates for

307   the air-sea gas exchange (J$_{ex}$) and vertical mixing fluxes (F$_{mix}$) over the respective time interval

308   to isolate the NCP contribution to observed ΔO_2/Ar changes (Izett et al., 2018; Tortell et al.,

309   2014). A negative J$_{ex}$ indicates net transfer of O$_2$ from the atmosphere to the mixed layer, while a

310   negative F$_{mix}$ indicates vertical transfer of ΔO_2/Ar-depleted to the mixed layer, both in units of

311   mmol m$_{-2}$ d$_{-1}$. Gross O$_2$ production rates were converted into carbon units using a photosynthetic

312   quotient (PQ) for new production of 1.4 for drifter period 1 calculations and a PQ for regenerated

313   production of 1.1 for drifter period 2 (Laws, 1991). Community respiration rates were converted

314   into carbon units using the same PQ values, and considered constant over each respective day

315   length period (i.e., $t_d + t_N$). This assumption of an equivalent respiratory quotient (RQ) and PQ

316   within each drifter period is reasonable given the wide range of respiration ratios reported in

317   prior studies across a range of oceanic environments (Anderson and Sarmiento, 1994; Robinson

318   and Williams, 1999; Robinson et al., 1999; Hedges et al., 2002; Robinson et al., 2002; Lønborg

319   et al., 2011; Daneri et al., 2012; Fernández-Urruzola et al., 2014). Moreover, Robinson and

320   Williams (1999) estimated lower RQ values at lower productivity stations in the Arabian Sea,

321   suggesting that it is reasonable to assume a lower RQ value (equivalent to PQ= 1.1) at drifter site

322   2.

323

324 $\quad NCP_{\frac{O2}{Ar},D\ or\ N} = z_{mld}\frac{dO_{2bio}}{dt}\Big|_{D\ or\ N} + J_{ex}|_{D\ or\ N} - F_{mix}$ (1)

325

326 $\quad GPP_{O2/Ar} = \dfrac{t_d(NCP_{\frac{O2}{Ar},D} - NCP_{\frac{O2}{Ar},N})}{PQ(t_d+t_N)}$ (2a)

327 $\quad CR_{O2/Ar} = \dfrac{NCP_{\frac{O2}{Ar},N}}{PQ(t_d+t_N)}$ (2b)

328 $\quad NCP_{\frac{O2}{Ar},24hr} = \dfrac{t_d NCP_{\frac{O2}{Ar},D} + t_N NCP_{\frac{O2}{Ar},N}}{PQ(t_d+t_N)}$ (2c)

329

330 $\quad O_{2bio} = \Delta\dfrac{O_2}{Ar}\dfrac{1}{100\%}O_{2eq}$ (3)

331

332 $\quad J_{ex} = k_{o2}O_{2bio}$ (4)

333

334 $\quad F_{mix,O2/Ar} = k_{mix}\dfrac{dO_{2bio}}{dz} = k_{N2O}N_2O_{bio}\dfrac{dO_{2bio}}{dN2O_{bio}}$ (5)

335

336 $\quad k_{mix} = k_{N2O}N_2O_{bio}(\dfrac{dN2O_{bio}}{dz})^{-1}$ (6)

337

338 $\quad N_2O_{bio} = N_2O_{meas} - N_2O_{eq} - N_2O_{thermal}$ (7)

339

340   Equilibrium concentrations of O_2 and N_2O ([O_2]$_{eq}$ and [N_2O]$_{eq}$) were calculated using the

341 salinity and temperature-dependent equations of Garcia and Gordon (1992) and Weiss and Price

342 (1980), respectively, and sea surface temperature and salinity from the ship's thermosalinograph.

343 Estimates of surface excess N_2O saturation, [N_2O]$_{bio}$, included a heat flux correction to account

344 for solubility changes (Keeling and Shertz, 1992; Jin et al., 2007; Izett et al., 2018). Non-

345 weighted piston velocities (k_{O2} and k_{N2O}; units of m d^{-1}) were calculated using the diffusive air

346 sea gas flux and Schmidt number parameterizations of Wanninkhof (2014) and Raymond et al.

347 (2012), and ship-based wind speed data 10 m above the sea surface. Daytime and nighttime

348 estimates for the gas exchange term, J_{ex}, were calculated using day/night average [O_2]$_{eq}$, $\Delta O_2/Ar$,

349 and k_{O2} values. Vertical gas gradients ($\frac{dN2O_{bio}}{dz}$ and $\frac{dO_{2bio}}{dN2O_{bio}}$) were estimated from our discrete

N$_2$O measurements and Rosette O$_2$ profiles over the upper 100 m of the water column, following Izett et al. (2018).

At drifter site 1, daily F$_{mix}$ values were calculated using daily [N$_2$O]$_{bio}$, daily vertical gradient and daily average k$_{N2O}$ values, and converted to carbon units using a PQ of 1.4. Denitrification should not have been a source of N$_2$O within the upper 100 m of the water column because measured O$_2$ concentrations were consistently greater than the threshold value of ~50 mmol m$_{-3}$ (e.g., Hopkinson and Barbeau, 2007). Likewise, we assumed no lateral advection of N$_2$O into drifter site 1, as there were little differences in the mixing ratio [O$_2$]$_{bio}$/[N$_2$O]$_{bio}$ across profile measurements (Fig. S2). While the August 22 CTD cast did exhibit a more anomalous [O$_2$]$_{bio}$/[N$_2$O]$_{bio}$ profile relative to the other two cast profiles, inclusion of these data had little impact on the vertical mixing correction. At drifter site 2, we assumed that vertical mixing was negligible due to the presence of strong density stratification, and therefore did not calculate a mixing flux correction at this site. In any case, the presence of a sub-surface O$_2$ maximum (Fig. S2) at this site would limit the application of the N$_2$O correction (Izett et al., 2018).

2.6.2 Optically-derived rates

We used the approach of Claustre et al. (2008) and White et al. (2017) to calculate daily-integrated GPP$_{POC}$, CR$_{POC}$, and NCP$_{POC}$ from daytime and nighttime changes in POC (dPOC/dt), derived from linear regressions of POC concentrations against time through day and night intervals. In certain ocean environments, NCP$_{POC}$ will not equate to NCP$_{O2/Ar}$ as a result of additional POC sinks, including export, grazing and DOC production. Under these conditions, CR$_{POC}$ includes these loss terms, and therefore NCP$_{POC}$ more accurately reflects net POC accumulation, as will be discussed further in Sect. 4. Nonetheless, for consistency with previous studies, we use the term NCP$_{POC}$ to describe the quantities computed in Eq. 8.

$$NCP_{POC,D\ or\ N} = z_{mld} \left.\frac{dPOC}{dt}\right|_{D\ or\ N} - F_{mix(POC)} \tag{8}$$

$$GPP_{POC} = \frac{t_d(NCP_{POC,D} - NCP_{POC,N})}{t_d + t_N} \tag{9a}$$

380 $\quad CR_{POC} = \frac{NCP_{POC,N}}{t_d + t_N}$ (9b)

381 $\quad NCP_{POC,24hr} = \frac{t_d NCP_{POC,D} + t_N NCP_{POC,N}}{t_d + t_N}$ (9c)

382

383 The presence of significant upwelling at drifter site 1 provides additional complexity in the

384 estimate of NCP from optically-derived POC measurements. In particular, vertical transport of

385 particle-deficient seawater from below the mixed layer into the surface could dilute the c_P signal

386 used to derive POC concentrations (Stramska and Dickey, 1994). To address this, we applied the

387 vertical mixing term, k_{mix}, derived from Eq. (6) to estimate the average daily dilution effect on

388 mixed layer POC concentrations through drifter period 1:

389

390 $\quad F_{mix,POC} = k_{mix} \frac{dPOC}{dz}$ (10)

391

392 A negative $F_{mix,POC}$ indicates transfer of [POC]-deficient seawater into the mixed layer. The term

393 d[POC]/dz represents the vertical gradient in [POC], derived from daily average POC

394 concentrations measured in Rosette samples at 5 m and near the base of the euphotic zone, below

395 the mixed layer (40–60 m) (Sect. 2.4). The dz term was calculated as the difference between the

396 average mixed layer depth from all CTD casts and the daily average shallowest depth of

397 minimum particle concentrations based on beam transmission profiles. At drifter site 2, $F_{mix,POC}$

398 was considered negligible (Sect. 2.6.1) due to the high density stratification of the water column.

399 $\quad$ In total, three sets of 24-hour GPP, CR and NCP values were calculated during the drifter

400 1 deployment from the three pairs of consecutive day and night intervals, starting with the first

401 night interval and ending with the last day interval. We excluded the first day-time interval from

402 our calculations, due to the erratic salinity values observed during the first day of this drifter

403 deployment (Sect. 3.1; Fig. S3). Because the drifter period was terminated prior to sunset, the

404 last day interval was 1.6 hours shorter than the average daytime duration. For the second drifter

405 deployment, two sets of GPP, R and NCP values were calculated from consecutive day and night

406 intervals, starting with the first daytime interval and ending with the last nighttime interval. The

407 initiation of the drifter period occurred after sunrise, so the first day interval was 1.1 hours

408 shorter than the average daytime duration.

409

410   **2.6.3 Integration time scales**

411

412   The approach to calculating NCP on the basis of linear regressions utilizes the high

413   temporal resolution of our data set. We compared our results from Sects. 2.6.1 and 2.6.2 to NCP

414   values calculated using several of other integration time scales. Following studies that have

415   calculated daily NCP values from "instantaneous" rates of change (e.g., hourly rates in Hamme

416   et al. (2012) and Tortell et al. (2014)), we divided our NCP calculations into shorter increments.

417   Given that the average measurement interval was ~15 minutes (after removing values where the

418   ship was not sufficiently close to the drifter; Sect. 2.1), we calculated NCP within three-hour

419   intervals:

420

421    $$NCP_{\frac{O2}{Ar},3hr} = \frac{3}{24}\left[z_{mld}\left(\frac{dO_{2bio}}{dt}\right)_{3hr} + J_{ex,3hr}\right]/PQ \qquad (11a)$$

422    $$NCP_{POC,3hr} = z_{mld}\left[\frac{3}{24}\left(\frac{dPOC}{dt}\right)_{3hr}\right] \qquad (11b)$$

423

424   For each day of the drifter periods, eight consecutive three-hour NCP values were summed into a

425   24-hour period to yield daily NCP estimates. We then applied the vertical mixing correction to

426   these daily estimates (refer to Eqs. 5, 6, 10), since the correction was only available on a daily

427   basis given the lower sampling resolution of [N_2O] and [POC] profiles. We also calculated daily

428   NCP using the difference between $\Delta O_2/Ar$ or [POC] between two time points at the beginning

429   and end of each 24-hour period (similar to the approach in Alkire et al. (2012); and Barnes and

430   Antoine (2104)). Finally, we calculated a single daily NCP rate per drifter period using the linear

431   regression of $\Delta O_2/Ar$ and [POC] against time over the entire drifter deployment. For these latter

432   two approaches, the 24-hour average and drifter-period average of relevant terms in Eqs. 1-9

433   were used to calculate NCP, and a PQ was used to convert O_2 to carbon units.

434

435   **2.7 Error analysis**

436

437   Errors for all estimates of net primary productivity (CbPM-NPP, 14C-NPP) and net

438   community production (NCP$_{O2/Ar}$, NCP$_{POC}$) were propagated from uncertainties associated with

439   all variables used for the computations. Error estimates for time-averaged variables were

440 generally represented by the standard deviation, as we assumed that this significantly exceeded

441 the error of the individual measurements prior to averaging. The uncertainty in z_{mld}, derived from

442 the standard deviation of mixed layer depths across individual CTD casts, was 2 m for drifter site

443 1 and 5 m for drifter site 2 (Sect. 2.3). Small uncertainties in t_D and t_N were calculated as the

444 standard deviations of all day or night lengths measured during both drifter periods (0.14 and

445 0.10 hours, respectively). Mean relative errors of [Chl-a] and [C_{ph}] from Burt et al. (2018), and

446 mean relative standard deviations in MODIS-derived daily surface PAR values were propagated

447 to calculate the error in CbPM-NPP. The standard deviations of triplicate 24-hour ^{14}C uptake

448 incubations were propagated to calculate the error in ^{14}C-NPP estimates. The uncertainties in

449 ^{14}C-NPP values are likely underestimated, as they do not account for bottle effects, as discussed

450 in Sect. 4.3.

451   For calculating error in NCP, uncertainties in dO_{2bio}/dt and $dPOC/dt$ were derived from

452 the confidence interval of the best-fit slope of linear regression of each variable against time.

453 Standard deviations of averaged $\Delta O_2/Ar$, k_{O2}, and k_{N2O} values, and the mean relative errors of

454 [N_2O]$_{meas}$, [N_2O]$_{Eq}$, [N_2O]$_{thermal}$, and $\frac{dO_{2bio}}{dN2O_{bio}}$ reported in Izett et al. (2018), were propagated into

455 the mixing correction errors for $NCP_{O2/Ar}$ and NCP_{POC}. The error in $\frac{dN2O_{bio}}{dz}$ was calculated as the

456 confidence interval of the best fit slope extracted from a linear regression of pooled drifter 1

457 [N_2O]$_{bio}$ values against depth. In propagating the error associated with the $dPOC/dz$ term in Eq.

458 10, we have included the standard deviation of the minimum transmissivity depth across daily

459 CTD casts and the standard deviation of POC measured in multiple blank combusted filters

460 (Sect. 2.4). Finally, to account for variability in the PQ and RQ, we assumed an uncertainty of

461 0.1, following the range reported Laws (1991).

462

463 **3 Results**

464

465 **3.1 Water mass properties**

466

467   Ship-board underway measurements revealed clear differences in hydrographic and

468 biogeochemical characteristics between the water masses sampled by the two drifters. Surface

469 water properties at drifter site 1 reflected the presence of a recently upwelled water mass that was

470   relatively cold (11.8 ± 0.4 °C), saline (32.6 ± 0.04 g/kg), and nutrient-rich (Figs. 1, S3, S4). The

471   Pacific Fisheries Environmental Laboratory's coastal upwelling index at 45°N, 125°W was

472   positive throughout drifter period 1. In contrast, the water mass tracked by the second drifter

473   deployment was warmer (17.5 ± 0.1°C) and fresher (31.8 ± 0.05 g/kg), with lower average mixed

474   layer nutrient concentrations.

475   Examination of surface water hydrographic properties during the two drifter deployments

476   suggest that both drifters tracked a relatively homogenous water mass, excluding a period of

477   salinity variability during the first day of drifter deployment 1, and several transient temperature

478   and salinity excursions after the second night of this deployment (grey patches in Fig. S3). These

479   features indicate potential intrusion of external water masses, possibly a result of loss of the

480   drifter drogue (Sect. 2.1). Observations during these periods were thus removed from the data set

481   prior to analysis. Outside of these intervals, variability in salinity (drifter 1: 32.5–32.7 g/kg;

482   drifter 2: 31.8–31.9 g/kg) was small during both drifter deployments. Variability in sea surface

483   temperature was also limited (drifter 1: 11.2–13.0 °C, drifter 2: 17.3–17.7 °C), and largely

484   reflected a diurnal variation of warming and cooling, which was particularly evident for drifter

485   period 2.

486   Temporal differences in CTD cast profiles point to some variation in mixed layer depth

487   (z_{mld}) during both drifter deployments. In general, there were no multi-day trends or regular

488   diurnal patterns in z_{mld} through both periods, suggesting that transient shifts in water column

489   turbulence likely contributed to changes in the shape of temperature, salinity, dissolved oxygen

490   and fluorescence profiles. Average z_{mld} values, calculated over each drifter period, had relatively

491   low relative standard deviations (<25%) and were applied to all subsequent calculations (Sect.

492   2.3). A sensitivity analysis, not shown, indicated that the choice of mixed layer depth using

493   different criteria (i.e., fluorescence profiles, density profiles and the density difference criterion)

494   and different time scales of integration (i.e., daytime/nighttime, 24 hour, and multi-day) did not

495   significantly impact the results discussed below.

496   Average mixed layer nutrient concentrations fluctuated during both drifter deployments,

497   but did not exhibit regular diurnal cycles (Fig. S4). At drifter site 1, concentrations ranged from

498   0.74 to 0.85 µM phosphate, 7.8 to 9.0 µM nitrate and nitrite, and 9.2 to 11.1 µM dissolved silica,

499   excluding day 1 of the drifter deployment and anomalously high concentrations measured during

500   a noisy CTD cast at midnight on the last day of the deployment. Excluding these outliers, a

501 significant (p<0.05) linear regression of each nutrient concentration against time revealed that

502 phosphate concentrations decreased by ~0.07 µM, [NO_3^- + NO_2^-] decreased by 0.9 µM, and

503 [SiO_2] decreased by 1.2 µM over the three-day drifter period, roughly in Redfield ratio

504 proportions (Sect. 3.4). Nutrient concentrations varied less at site 2, from 0.08–0.10 µM [PO_4^{3-}],

505 0.29–0.61 µM [NO_3^- + NO_2^-], and 1.2–1.7 [SiO_2]. While [PO_4^{3-}] and [SiO_2] increased

506 significantly (p<0.05) by 0.015 µM and 0.48 µM, respectively, these changes were small

507 compared to the nutrient drawdown observed during drifter period 1, and did not reflect Redfield

508 ratio proportions. It is possible that intrusions of an external water mass with slightly elevated

509 nutrient concentrations contributed to the small increase in [PO_4^{3-}] and [SiO_2] measured during

510 these CTD casts, even though we assume that such effects on our derived productivity estimates

511 are negligible based on inspection of underway temperature and salinity data (Fig. S3).

512

513 **3.2 Biogeochemical comparisons between drifter sites**

514

515 Elevated nutrient concentrations at the drifter 1 site supported high productivity and the

516 accumulation of phytoplankton biomass, as indicated by elevated chlorophyll-a ([Chl-a]= 0.66–

517 1.5 µg/L), phytoplankton carbon ([C_{ph}]= 83–115 µg/L) and particulate organic carbon

518 concentrations ([POC]= 130–261 µg/L) (Figs. 2a–c). We observed [C_{ph}]/[Chl-a] ratios ranging

519 from 68–143 g/g, with a median value of 85 g/g (Fig. 2f). Using the carbon-based production

520 model (CbPM; Sect. 2.5) and daily-averaged mixed layer PAR derived from satellite values

521 matched to drifter location (within 5 km), these [C_{ph}]/[Chl-a] ratios translate into phytoplankton

522 growth rates ranging from 0.75–0.94 d$_{-1}$. At the second drifter site, phytoplankton productivity

523 and biomass were significantly lower in the nutrient-poor waters ([Chl-a]= 0.06–0.21 µg/L,

524 [C_{ph}]= 11–17 µg/L, and [POC]= 25–38 µg/L). Ratios of [C_{ph}] to [Chl-a] at site 2 were

525 significantly higher (p<0.05) than those observed at site 1, ranging from 69 g/g to 203 g/g, with a

526 median value of 108 g/g. The higher ratios may reflect reduced cellular [Chl-a] associated with

527 greater nutrient limitation, higher daily-integrated PAR, and proportionally more picoplankton

528 than microplankton at drifter site 2 (Westberry et al., 2008; Hirata et al., 2011; Graff et al., 2016;

529 Burt et al., 2018). Median PAR levels were higher and less variable at site 2, in part contributing

530 to lower variability in CbPM-based growth rates, which ranged from 0.81 to 0.85 d$_{-1}$.

531   Several lines of evidence suggest that the phytoplankton assemblage at drifter site 1 was

532   enriched in large-celled phytoplankton, as compared to drifter site 2. The wavelength-dependent

533   slope of particulate backscatter (b_{bp}) was lower at site 1 (range: 1.4 to 1.6, median: 1.5) than at

534   site 2 (range: 1.9–2.3, median: 2.1) (Fig. 2d), suggesting proportionally larger particle sizes

535   (Stramska et al., 2003; Kostadinov et al., 2009). This observation is supported by size-

536   fractionated Chl-a measurements. During the drifter 1 deployment, the >20 µm size fraction

537   (Sect. 2.4), increased from 21 % to 46 % of the total Chl-a pool, indicating the enrichment of

538   large phytoplankton in the assemblage. Pigment-based estimates of phytoplankton taxonomic

539   composition and size class (Hirata et al., 2011; Zeng et al., 2018) suggested that relative diatom

540   and microplankton abundances exceeded 50% on the final sampling time point. By comparison,

541   size-fractionated [Chl-a] and HPLC analyses from drifter 2 indicated a lower proportion of large-

542   celled phytoplankton, with 9–15% of total [Chl-a] in the >20 µm size fraction, and diatoms and

543   micro-plankton estimated to account for 19–29% of the phytoplankton assemblage. The

544   proportion of picoplankton increased through time at drifter site 2 from 31–50% of total [Chl-a],

545   alongside a slight increase in b_{bp} slope, indicating accumulation of smaller particle sizes (Fig.

546   S3d). Finally, median bulk refractive index values across three wavelengths (470 nm, 532 nm,

547   650 nm) were higher at site 1 (1.08–1.11) than at site 2 (1.02–1.04) (Fig. S3e), which is

548   consistent with a greater proportion of diatom-derived silica in the particle pool (Lide, 1997;

549   Twardowski et al., 2001).

550

551   **3.3 Diurnal variability and primary production**

552

553   As shown in Fig. 3a, clear diurnal cycles in biological oxygen saturation ($\Delta O_2/Ar$) were

554   observed during both drifter deployments. Generally, values of $\Delta O_2/Ar$ increased from dawn to

555   dusk and decreased from dusk to dawn, yielding positive slopes of linear regressions of $\Delta O_2/Ar$

556   against time in the daytime, and negative slopes at night. During drifter deployment 1, this

557   diurnal cycle was superimposed on a longer-term increase in biological O_2 saturation as under-

558   saturated values returned toward atmospheric equilibrium. At least part of this increase is

559   attributable to gas exchange, which would act to erase O_2 under-saturation in the mixed layer

560   caused by recent upwelling. However, calculation of the sea-air O_2 flux shows that, except for

561   the first 24-hour period, only a small amount of the daily increase in $\Delta O_2/Ar$ can be explained by

562 gas exchange (absolute value of $J_{ex} < 10$ mmol O_2 m^{-2} d^{-1}) (Table 1). Thus, the temporal change

563 in $\Delta O_2/Ar$ can be attributed to a primarily biological source. The magnitude of this increase is

564 further underestimated because of vertical upwelling of deep oxygen-poor waters, which would

565 act to dampen the increase in $\Delta O_2/Ar$ through time. After accounting for a mixing correction

566 ranging between 22 and 97 mmol m^{-2} d^{-1} O_2 (equivalent to 16 to 70 mmol m^{-2} d^{-1} C when

567 assuming a photosynthetic quotient of 1.4), daily-integrated gross primary productivity

568 (GPP$_{O2/Ar}$) ranged from 270 to 358 mmol C m^{-2} d^{-1}, and community respiration (CR$_{O2/Ar}$) rates

569 ranged from 74 to 172 mmol C m^{-2} d^{-1} (Table 1).

570   Examination of the diel variability in POC and Chl-a during drifter period 1 revealed

571 significant differences in the behavior of these variables as compared to $\Delta O_2/Ar$ (Fig. 3b, c). In

572 particular, while $\Delta O_2/Ar$ increased during the first drifter deployment, [POC] and [Chl-a] values

573 decreased. We estimated that vertical mixing (F$_{mix,POC}$), accounted for 12 to 68 mmol m^{-2} d^{-1} C of

574 these daily changes in [POC], similar to the magnitude of the mixing correction for $\Delta O_2/Ar$

575 variability (Table 1). After taking mixing into account, daily-integrated GPP$_{POC}$ decreased from

576 242 mmol m^{-2} d^{-1} on day 1 to 98 mmol m^{-2} d^{-1} on day 3, while CR$_{POC}$ rates ranged from 77 to

577 147 mmol m^{-2} d^{-1}.

578   Calculated daily averaged net primary productivity (NPP) were lower than GPP$_{O2/Ar}$.

579 Rates derived from the CbPM model (Sect. 2.5), declined from 147 mmol C m^{-2} d^{-1} on day 1 of

580 drifter deployment 1 to 112 mmol C m^{-2} d^{-1} on day 3 (Table 1), reflecting the trend in Chl-a

581 concentrations used to derive NPP (Fig. 3c). The CbPM-derived NPP estimates were similar to

582 that obtained in 14C incubations (150 ± 18 mmol C-m^{-2}d^{-1}) within the first 24 hours of drifter

583 deployment 1. However, 14C-based NPP estimates on the third day of the deployment (49 ± 8

584 mmol C-m^{-2}d^{-1}) were about two-fold lower than those obtained from CbPM calculations.

585   Dissolved oxygen and POC dynamics at drifter site 2 differed significantly from those

586 observed at site 1. Compared to the drifter site 1, diel variability in $\Delta O_2/Ar$ and [POC] was more

587 tightly coupled during the second drifter deployment (Fig. 3a, b). Both O_2/Ar and [POC]

588 displayed regular diurnal variations, increasing in the daytime to a maximum around dusk and

589 decreasing at night to a minimum around dawn. Over the full drifter deployment, concentrations

590 of Chl-a and, to a lesser extent, POC, decreased, in contrast to $\Delta O_2/Ar$, which remained relatively

591 constant across days. Daily-integrated GPP$_{O2/Ar}$ values ranged from 108 to 219 mmol C m^{-2} d^{-1}

592 and CR$_{O2/Ar}$ rates ranged from 82 to 186 m^{-2} d^{-1}. POC-derived values were considerably lower

593 and less variable, from 41 to 38 for GPP$_{POC}$ and 36 to 44 for CR$_{POC}$ (Table 1). NPP derived from

594 CbPM calculations was 22 mmol C m^{-2} d^{-1} on the first day of the drifter period and 18 mmol C

595 m^{-2} d^{-1} on the second day, while NPP calculated from one ^{14}C bottle incubation during the first

596 day of the drifter 2 deployment was 12 ± 4 mmol C m^{-2} d^{-1}, showing good agreement with the

597 CbPM calculations.

598

599 **3.4 Net community production**

600

601   Daily net community production (NCP) rates were calculated using linear regressions of

602 $\Delta O_2/Ar$ and POC over day and night intervals, corrected for gas exchange and vertical mixing

603 (Sect. 2.6.1, 2.6.2). During drifter period 1, NCP$_{O2/Ar}$ and NCP$_{POC}$ exhibited contrasting trends, as

604 NCP$_{O2/Ar}$ remained >100 mmol C m^{-2} d^{-1} throughout, while NCP$_{POC}$ declined to negative values

605 on the second and third days (Table 1; Fig. 4). The transition to negative NCP$_{POC}$ values over the

606 course of the drifter 1 deployment primarily reflected diminishing daytime rates of POC

607 accumulation (dPOC/dt term in Eq. 8). At drifter period 2, we observed closer agreement

608 between NCP values. $\Delta O_2/Ar$-derived NCP ranged from -12 to 33 mmol C m^{-2} d^{-1} over two

609 consecutive 24 hour periods, while NCP$_{POC}$ values ranged from -3 to 1 mmol C m^{-2} d^{-1}. These

610 lower rates at drifter site 2 are consistent with the lower observed phytoplankton biomass and

611 nutrient concentrations.

612   Additional constraints on NCP during drifter period 1 can be derived from examining

613 nutrient drawdown. Because vertical upwelling of nutrient-replete waters would dampen the

614 magnitude of observed nutrient drawdown over time (Sect. 3.1; Fig. S4), we used the derived

615 k$_{mix}$ from Eq. 6 and a best-fit vertical gradient in nutrient concentrations between the mixed layer

616 and 100 m (Sect. 2.4) to account for this mixing flux. This correction increases the cumulative

617 three-day nutrient drawdown by 2.1 to 2.6 times. Over the three-day drifter deployment, surface

618 Si, N and P concentrations declined in a ratio of 17: 13: 1, which is consistent with the

619 stoichiometry expected for organic matter produced by a diatom-rich assemblage (Brzezinski et

620 al., 1998; Turner et al., 1998; Brzezinski, 2004). Assuming that the observed decrease in SiO$_2$

621 concentrations over the three days is attributable to growth of diatoms in the mixed layer, and

622 applying a stoichiometric ratio of 106 C: 16 Si, we estimate an average C production rate of

623 ~128 mmol C m^{-2} d^{-1} for the drifter period. This value is consistent with NCP$_{O2/Ar}$ rates, which

624 were 137 mmol C m-2 d-1 on average over three days, but significantly greater than NCP$_{POC}$

625 estimates (7 mmol C m-2 d-1 on average) (Table 2).

626   Table 2 summarizes comparisons among NCP values calculated using day/night linear

627 regressions of $\Delta O_2/Ar$ and POC against time, and other approaches described in Sect. 2.6.3. In

628 general, the different calculation methods did not significantly alter the results. NCP values

629 derived from one linear regression over each drifter period agreed well with the average of two

630 (drifter 2) to three (drifter 1) daily NCP values calculated via the other approaches. Small

631 differences between linear regression-based NCP values and both NCP calculated from either 3-

632 hour increments or two time points are likely due to the effect of lower signal to noise in $\Delta O_2/Ar$,

633 [O$_2$]$_{bio}$ and [POC] values utilized in these latter two approaches. The following discussion thus

634 focuses on productivity rates derived from day/night linear regressions (i.e., Eqs. 1 and 8), which

635 utilize all data points while minimizing uncertainty in the derived rates of change. The exception

636 is the NCP$_{O2/Ar}$ value calculated for day 1 of drifter period 2 using the daytime/nighttime linear

637 regression method. By this approach, we calculated NCP$_{O2/Ar}$ as 26 mmol C m-2 d-1, even though

638 the time series in Fig. 3a clearly indicates a net decrease in $\Delta O_2/Ar$ over the 24-hour period, and

639 all other $\Delta O_2/Ar$-based NCP calculations (Sect. 2.6.3) yielded negative values. For the

640 discussion, Table 1 and Fig. 4, the NCP value derived from the integrated 3-hour increments

641 represents net community production during this particular interval.

642

643 **4 Discussion**

644

645   A number of previous studies have examined diurnal variation in upper ocean

646 phytoplankton and organic particle dynamics across a variety of productivity regimes, from

647 oligotrophic environments (Claustre et al., 1999, 2008; Wu et al., 2010; Gernez et al., 2011;

648 Kheireddine and Antoine, 2014; Thyssen et al., 2014; Nicholson et al., 2015; Ribalet et al., 2015;

649 White et al., 2017), to higher productivity waters and phytoplankton blooms (Brunet and Lizon,

650 2003; Wu et al., 2010; Gernez et al., 2011; Alkire et al., 2012; Dugenne et al., 2014; Kheireddine

651 and Antoine, 2014; Needham and Fuhrman, 2016; Briggs et al., 2018). In general, these studies

652 have shown that more productive environments exhibit higher amplitude diurnal variations in

653 beam attenuation, POC concentration, phytoplankton cell abundances, Chl-a, and metabolic

654 rates. These prior results are consistent with the differences we observed between the two

655 distinct Northeast Pacific trophic environments represented by drifter sites 1 and 2, respectively

656 (Sect. 3.2; Fig. 2).

657 Biogeochemical properties during the first Lagrangian survey suggested a dynamic,

658 highly productive phytoplankton community, influenced by upwelling and elevated mixed layer

659 nutrient concentrations (Figs. 1, S4). Several lines of evidence imply the presence of a

660 developing diatom bloom at this site (Sect. 3.2; Figs. 2, 3). Increasing mixed layer biological

661 oxygen saturation ($\Delta O_2/Ar$) was contrasted by a general decrease in particulate organic carbon

662 (POC) concentrations, suggesting a significant decoupling between O_2 and POC dynamics. This

663 was reflected in significant differences between $\Delta O_2/Ar$-derived gross primary productivity

664 (GPP) and net community production (NCP) rates derived from $\Delta O_2/Ar$ and POC measurements

665 (Figs. 4, 5; Table 1). In contrast, biogeochemical properties during the second drifter deployment

666 were indicative of a lower productivity, nutrient-limited phytoplankton assemblage, with near-

667 zero $\Delta O_2/Ar$ values reflecting a close balance between water column photosynthesis and

668 respiration (Fig. 3a). Relative to the drifter 1 site, diurnal variations in $\Delta O_2/Ar$ and POC were

669 more closely coupled, while phytoplankton biomass (C_{ph}) and chlorophyll-a (Chl-a)

670 concentrations (dominated by smaller cells) varied little through time. Contrary to our

671 expectations, even though $NCP_{O2/Ar}$ and NCP_{POC} rates agreed well, we also observed significant

672 discrepancies between $GPP_{O2/Ar}$ and GPP_{POC} and between $CR_{O2/Ar}$ and CR_{POC} during drifter

673 period 2. The contrasting properties between the two drifter deployments enable us to examine

674 the coupling of O_2 and POC dynamics under different ecological states, with implications for the

675 use of $\Delta O_2/Ar$ and POC measurements as proxies for GPP and NCP.

676

4.1 Decoupling of O_2 and POC dynamics in the mixed layer

678

679 **4.1.1. Drifter 1.** In the absence of significant POC sinking and net loss to the dissolved

680 organic carbon (DOC) pool, POC-based productivity rates should approximate $\Delta O_2/Ar$-based

681 rates (Claustre et al., 2008; White et al., 2017). However, at drifter station 1, both $GPP_{O2/Ar}$ and

682 $NCP_{O2/Ar}$ greatly exceeded GPP_{POC} and NCP_{POC}, respectively (Figs. 4, 5a; Table 1). Over the

683 three successive 24-hour periods of drifter deployment 1, the absolute difference between GPP

684 measures increased from 41 mmol C m$_{-2}$ d$_{-1}$ to 260 mmol C m$_{-2}$ d$_{-1}$, while the absolute difference

685 between NCP estimates increased from 42 mmol C m$_{-2}$ d$_{-1}$ to 193 mmol C m$_{-2}$ d$_{-1}$. This

686 discrepancy exceeded the propagated NCP uncertainties during the second and third days of the

687 deployment, and was apparent in all approaches used to calculate NCP (Sect. 2.6.3, Table 2).

688 While mixed layer $\Delta O_2/Ar$ primarily reflected O_2 accumulation from GPP and O_2 loss

689 from CR, diurnal variability in [POC] was likely affected by several additional loss factors,

690 which are discussed below. The variable difference between O_2-based and POC-based NCP

691 measured over 3-hour increments (Eq. 11; Fig. S5) suggests that apparent POC loss rates were

692 variable throughout the drifter period, and lower at night relative to day. Thus, the higher

693 $NCP_{O2/Ar}$ may be attributed more to differences in daytime accumulation of POC and O_2 rather

694 than differential POC and O_2 losses at night. Indeed, we found that differences between $CR_{O2/Ar}$

695 and CR_{POC} were smaller than differences in NCP or GPP throughout drifter period 1, and $CR_{O2/Ar}$

696 exceeded CR_{POC} during two of three nights (Fig. 5b).

697 In the dynamic, high productivity upwelling environment of drifter site 1, a number of

698 processes can account for variable POC loss rates on various time scales (Gardner et al., 1999;

699 White et al., 2017; Briggs et al., 2018). During a diatom bloom, enhanced aggregation of large

700 silica-rich particles and zooplankton fecal pellet production can stimulate POC export and

701 diatom cells out of the mixed layer (Buesseler, 1998; Guidi et al., 2009; Brzezinski et al., 2015;

702 Stukel et al., 2017), progressively decreasing NCP_{POC} relative to $NCP_{O2/Ar}$. The discrepancy we

703 observed between NCP_{POC} and $NCP_{O2/Ar}$ (up to 193 mmol C m$_{-2}$ d$_{-1}$) is in the upper range of

704 prior export estimates from various oceanic regions, including the Southern Ocean (~83 mmol C

705 m$_{-2}$ d$_{-1}$), North Atlantic spring bloom (96 mmol C m$_{-2}$ d$_{-1}$) and Southern California Current

706 system (~36 mmol C m$_{-2}$ d$_{-1}$) (Henson et al., 2012; Alkire et al., 2012; Stukel et al., 2017),

707 suggesting that POC export fluxes could comprise a significant fraction of the inferred POC loss

708 at drifter site 1. At the same time, sub-daily changes in particle sinking velocities and size

709 distributions could cause daytime export to exceed nighttime export (DuRand and Olson, 1998;

710 Waite and Nodder, 2001; Oubelkheir and Sciandra, 2008; Khierrediene and Antoine, 2014;

711 Ribalet et al., 2015; Briggs et al., 2018), leading to greater differences between $GPP_{O2/Ar}$ and

712 GPP_{POC} than between $CR_{O2/Ar}$ and CR_{POC}, as we observed.

713 Another likely POC loss is DOC production through cellular exudation, viral lysis and/or

714 grazing (Karl et al., 1998; Lochte et al., 1993; Claustre et al., 2008; Dall'Olmo et al., 2011;

715 Briggs et al., 2018). On daily time scales, this loss term would lower NCP_{POC} relative to

716 $NCP_{O2/Ar}$, provided that DOC production exceeds DOC respiration. Further, higher daytime net

717 DOC production would cause $GPP_{O2/Ar}$ to increase more than GPP_{POC} in the daytime, while a

718 decrease at night would cause $CR_{O2/Ar}$ to exceed CR_{POC} (Karl et al., 1998). Light- and

719 productivity-dependent increases in DOC production in the daytime, could result, for example,

720 from the effects of photo-respiration and other mechanisms of dissipating excess light energy

721 (Schuback and Tortell, 2019). While we did not conduct direct measurements of DOC

722 concentrations during the cruise, previous work in a variety of ocean environments has shown

723 that DOC production can account for 3-37% of NCP in the Ross Sea, up to 10-40% in the

724 equatorial Pacific Ocean, up to 66% in the Sargasso Sea during the seasonal phytoplankton

725 bloom, and 22-40% during the North Atlantic bloom (Hansell and Carlson, 1998; Alkire et al.,

726 2012). In the eastern Subarctic Pacific, Bif and Hansell (2019) estimated springtime ΔDOC/NCP

727 ratios of 0.05 – 0.54 and summertime ratios of 0 – 0.28 along the Line P transect (130 – 152

728 °W).

729   In addition, assuming that DOC exudation from phytoplankton cells is positively related

730 to growth in heterotrophic biomass (Fuhrman et al., 1985; Kuipers et al., 2000; Church et al.,

731 2004), variations in total bacterial biomass may have impacted c_P measurements at drifter site 1

732 (Oubelkheir and Sciandra, 2008; Gernez et al., 2011; Barnes and Antoine, 2014). If detected by

733 the ac-s sensor, bacteria could potentially account for some of the discrepancy between diel POC

734 and O_2-derived variability. In particular, c_P decreases from phytoplankton exudation would

735 counter c_P increases from heterotrophic growth. At night, this would decrease CR rates derived

736 from c_P-based [POC], relative to O_2-derived CR rates.

737   A final consideration involves diurnal variation of zooplankton abundances and grazing

738 rates, which could enhance POC loss without depleting $ΔO_2/Ar$ (Dall'Olmo et al., 2011; White et

739 al., 2017; Briggs et al., 2018), assuming that biomass accumulation rates from grazing surpass

740 grazer respiration rates (Dagg et al., 1982). Further, once POC is assimilated into the body of a

741 grazer, it joins a larger particle size class that likely exceeds the size-dependent detection limits

742 of the beam attenuation coefficient (Stramski and Kiefer, 1991; Marra, 2002; Claustre et al.,

743 2008;), decreasing the c_P signal used to derive POC. During our expedition, we observed a strong

744 signature of diel migrating zooplankton based on increased nighttime signal spikes in surface

745 optical backscatter measurements (Burt and Tortell, 2018). These effects would enhance CR_{POC}

746 relative to $CR_{O2/Ar}$, contrary to what we observed. We thus assume that grazing at drifter site 1 is

747 minimal relative to the effects of particle export and DOC production on GPP, CR and NCP.

748

749   **4.1.2 Drifter 2.** Relative to the drifter 1 site, drifter site 2 exhibited similar discrepancies

750   between $GPP_{O2/Ar}$ and GPP_{POC}, and greater discrepancies between $CR_{O2/Ar}$ and CR_{POC} (Fig. 5a-b;

751   Table 1). Irrespective of the time of day, the rate of $\Delta O_2/Ar$ change computed over 3-hour

752   intervals (Eq. 11) consistently exceeded POC-derived changes throughout the drifter period (Fig.

753   S5). The strong, positive relationship between these two 3-hour measures ($p<0.05$, $r_2=0.64$),

754   compared to the weaker correlation at drifter site 1 ($p<0.05$, $r_2= 0.39$) (Figs. 5c-d), suggests that

755   despite large differences in the magnitude of $\Delta O_2/Ar$-derived and POC-derived GPP and CR

756   rates, POC-based changes were a good relative indicator of O_2-derived productivity rates at

757   drifter site 2.

758   Because daytime increases in both $\Delta O_2/Ar$ and [POC] were balanced by nighttime

759   decreases, absolute differences in $NCP_{O2/Ar}$ and NCP_{POC} were smaller than at drifter site 1. This

760   result suggests a closer coupling between primary production and heterotrophic consumption, as

761   expected for this more oligotrophic ecosystem (Claustre et al., 2008; White et al., 2017). While

762   the NCP discrepancy was negligible over the first 24-hour period, it increased to 32 mmol C m-

763    $_2$d$_{-1}$ over the 24-hour period (Table 1; Fig. 4), exceeding the uncertainty of both NCP

764   calculations. This suggests low, but non-negligible, rates of particle export, grazing and/or net

765   DOC production at drifter site 2. Although we lack direct DOC measurements, this result is

766   consistent with several previous observations of low net DOC production in oligotrophic waters

767   (Bif et al., 2018; Hansell and Carlson, 1998), with values approaching ~30% of NCP in low

768   productivity offshore waters of the Subarctic Pacific (Bif and Hansell, 2019). Low particle

769   sinking rates could also explain the smaller absolute discrepancy between $NCP_{O2/Ar}$ and NCP_{POC}

770   at drifter site 2. Low particle export is generally expected from phytoplankton assemblages

771   dominated by small particle sizes <20µm, as evident in higher b_{bp} slope values and Chl-a size

772   fractionation measurements at drifter site 2 (Sect. 3.2; Fig. 2) (Fowler and Knauer, 1986; Guidi

773   et al., 2008).

774   Prior studies have observed that the amplitude of diurnal variability in $\Delta O_2/Ar$ exceeds

775   the amplitude of diurnal variability in c_p-based [POC], as we observed at drifter site 2 (Kinkade

776   et al., 1999; Hamme et al., 2012; Briggs et al., 2018). For example, Briggs et al. (2018) observed

777   higher amplitude variations in O_2 relative to c_p-derived [POC] during the North Atlantic bloom,

778   leading to higher absolute O_2-derived respiration and gross oxygen production (GOP) rates

779   compared to c_P-derived rates. In the Southern Ocean, Hamme et al. (2012) also observed high

780   ratios of underway $\Delta O_2/Ar$-derived gross oxygen production to gross carbon production (i.e.,

781   GPP) based on photosynthesis-irradiance incubations. As discussed above for drifter site 1, these

782   offsets between $\Delta O_2/Ar$ and POC-based measures might result from the effects of bacteria on c_P

783   measurements, especially at a relatively low productivity site like drifter site 2 (Table 1; Fig. 2)

784   (Claustre et al. 2008; Oubelkheir and Sciandra, 2008; Barnes and Antoine, 2014). Bacterial c_P

785   variability would act to counter phytoplankton c_P variability, decreasing the magnitude of CR_{POC}

786   relative to the magnitude of $CR_{O2/Ar}$. Indeed, the positive $CR_{O2/Ar}$ - CR_{POC} discrepancy at drifter

787   site 2 contributed to 58-82% of the differences between $\Delta O_2/Ar$ and POC-derived GPP rates. The

788   remaining difference may be attributed to greater daytime POC losses to the DOC pool and

789   through particle export.

790

791   **4.2 Other factors driving variability in NCP**

792

793   In interpreting our results, it is important to consider a number of methodological caveats

794   that could contribute to the apparent difference between $NCP_{O2/Ar}$ and NCP_{POC}. One important

795   variable in all of our comparisons of productivity rates is the O_2-to-POC conversion factor,

796   represented by the photosynthetic (PQ) and respiratory quotient (RQ). Given the relatively

797   narrow range of possible PQ values applicable to our study sites (~1.1-1.4) (Laws 1991),

798   variability in this term cannot account for the total discrepancy observed between $\Delta O_2/Ar$ and

799   POC-derived GPP, CR and NCP rates. By contrast, RQ values in the ocean are more variable

800   than PQ (Robinson and Williams, 1999; Robinson et al., 1999; Hedges et al., 2002). Therefore,

801   variability in RQ values at both drifter sites could introduce considerable uncertainty into

802    $GPP_{O2/Ar}$, $CR_{O2/Ar}$ and $NCP_{O2/Ar}$ calculations unaccounted for in our error propagations (Sect.

803   2.7). However, we found that use of RQ values ranging between 1.0 – 1.4 (Anderson and

804   Sarmiento, 1994; Robinson and Williams, 1999; Hedges et al., 2002; Daneri et al., 2012) did not

805   greatly change calculated $GPP_{O2/Ar}$, $CR_{O2/Ar}$, and $NCP_{O2/Ar}$ relative to GPP_{POC}, CR_{POC}, and

806   NCP_{POC}. Therefore, it is unlikely that our selected RQ values, 1.4 and 1.1 for drifter sites 1 and

807   2, respectively, biased our main interpretations.

808   In our analysis, we interpret variations in particulate backscatter (b_{bp}) and beam

809   attenuation (c_P) in terms of phytoplankton and total particulate organic carbon concentrations,

810   assuming a negligible influence of inorganic suspended minerals from various sources, including

811   sediment resuspension and transport by the Columbia River plume (Thomas and Weatherbee,

812   2006). This assumption is supported by the salinity of waters we sampled at both drifter sites,

813   which was significantly higher than that expected for river-influenced regions, (below 30 g/kg;

814   Hickey et al., 1998). At the same time, the observed bulk refractive index of particles (η_p) at

815   drifter site 1 do not preclude the presence of mixing between POC and a small fraction of shelf-

816   derived inorganic particles. Estimates of η_p were generally below 1.12 for this near-shore site

817   (Sect. 2.2; Fig. S3e), as compared to values as high as 1.26 for inorganic minerals in seawater

818   (Lide, 1997; Twardowski et al., 2001). By comparison, calculated η_p values during the drifter 2

819   deployment were below 1.08, which is much closer to values expected for water-containing

820   predominantly non-diatom phytoplankton organic carbon.

821   Additional uncertainty in our analysis derives from the algorithms used to estimate POC

822   and phytoplankton carbon C_{ph} from optical measurements (Sect. 2.2). Because of particle size

823   limitations in the optical measurements, they may not fully capture all significant size classes of

824   the particulate pool, such as larger microplankton and zooplankton. Such a size bias in the c_p

825   signal at 660 nm, used to derive [POC], would cause an underestimate of larger POC particles

826   measured by beam attenuation (Claustre et al., 2008; Marra, 2002; Stramski and Kiefer, 1991),

827   and thereby contribute to the apparent discrepancy between diel changes in [POC] and diel

828   changes in $\Delta O_2/Ar$. Despite these potential caveats, recent work (Graff et al., 2016; Briggs et al.,

829   2018; Burt et al., 2018) has demonstrated that c_p and b_{bp}-based derivations of [POC] and [C_{ph}]

830   can indeed be robust in high biomass ocean regions, where productivity and the proportion of

831   large-celled phytoplankton is significant.

832   Equally important, changes in the c_p-to-[POC] relationship through time could also drive

833   apparent variability in optical [POC] estimates. The linear regression of [POC] against c_p at 660

834   nm measured across diverse marine environments is defined over a range of POC concentrations

835   from ~5 to ~175 µg/L (Graff et al. 2015). At drifter site 2, POC concentrations fell within the

836   range of this fit, and particle properties that may influence POC/c_p values (i.e., b_{bp} slope values,

837   phytoplankton community composition, particle size and bulk refractive index) were relatively

838   constant through time (Figs. S3d, e). By comparison, POC concentrations at drifter station 1

839   were 25% higher than the empirical limits of the c_p-based algorithm in Graff et al. (2015),

840   requiring extrapolation of the POC/c_p relationship beyond its calibration range. In a limited

841 comparison with discrete POC samples, we found a POC–c_p slope that was similar to that of

842 Graff et al. (albeit with a different y intercept) (Fig. S1). Nonetheless, we cannot rule out changes

843 in the c_{p660}–[POC] relationship due to shifts in cell size and, to a lesser extent, bulk refractive

844 index resulting from diatom accumulation (Kheireddine and Antoine, 2014; Stramski and

845 Reynolds, 1993) (Fig. S3d–e). Indeed, Briggs et al. (2018) observed that the ratio of [POC] to c_p

846 decreased by ~20% during the rise of the North Atlantic bloom, while values increased by ~60%

847 during the bloom decline. If we assume a 20% decrease in POC/c_{p660} values (from ~420 to ~340

848 mg m$_{-2}$) associated with diatom growth (Briggs et al., 2018), our daily NCP$_{POC}$ estimates would

849 be less positive during day 1 and less negative during days 2–3. This, in turn, would increase the

850 apparent decoupling between NCP$_{POC}$ and NCP$_{O2/Ar}$ on days one (~27%) and three (~1%), and

851 bring the values slightly closer on day two (~8%). Overall, the value of these potential changes is

852 small relative to the differences we observed between NCP$_{O2/Ar}$ and NCP$_{POC}$, and we thus

853 conclude that variable POC/c_{p660} ratios cannot explain the observed decoupling between POC,

854 C_{ph} and dissolved O_2 dynamics at the drifter 1 site.

855   There are a number of other potential caveats in our analysis of phytoplankton carbon

856 from b_{bp} and particle size distribution from b_{bp} slope. Previous studies have reported that daily

857 variations in b_{bp} do not always track daily variations in c_p, suggesting that b_{bp} dynamics do not

858 reflect phytoplankton carbon dynamics on diel time scales (Kheireddine and Antoine, 2014;

859 Briggs et al., 2018). We observed a similar decoupling between b_{bp} and c_p in this study; for

860 example, while c_p values at 660 nm steadily declined in the last 24 hours of drifter period 1, b_{bp}

861 at 470 nm stayed relatively constant. Nonetheless, [C_{ph}] estimates from b_{bp} (Fig. 2) remain useful

862 for comparisons between drifter sites, and differences in apparent phytoplankton biomass

863 concentration were consistent with a number of the other biogeochemical differences measured

864 between the two trophic regimes. Similarly, the relationship between b_{bp} slope and particle size

865 distribution has been challenged in previous literature (e.g., Zeng et al., 2018). While this limits

866 our interpretation of daily b_{bp} slope dynamics, we did find independent evidence for larger

867 particle sizes at drifter site 1 (as predicted by the b_{bp} slope), from size fractionated [Chl-a]

868 measurements and pigment analysis showing a greater fraction of microplankton (Sect. 3.2).

869

870 **4.3 Reconciling NCP and NPP**

871

872   During both drifter surveys, we estimated daily-integrated net primary productivity

873   (NPP) values using carbon-based production model (CbPM) calculations and ^{14}C bottle

874   incubations (Sect. 2.5). On several days, these two estimates of NPP were consistently lower

875   than NCP$_{O2/Ar}$ integrated over the same time scales and mixed layer depths (Table 1). Similarly,

876   Briggs et al. (2018) and Alkire et al. (2012) also reported NCP values that were equal to or

877   greater than NPP values obtained from different methodologies during their Lagrangian study of

878   the North Atlantic Bloom.

879   In theory, NCP cannot exceed NPP, as NCP includes additional respiration terms not

880   included in NPP, and must always be equal to or (more realistically) lower than NPP. Recent

881   work in the Northeast Pacific Ocean, has reported mean NCP/NPP ratios, based on ΔO_2/Ar

882   measurements and CbPM calculations, ranging from 0.16 to 0.26 in offshore and coastal waters

883   (Burt et al., 2018). These values, determined from continuous observations along a moving ship-

884   track, are consistent with theoretical expectations. The observed high (>1) apparent NCP/NPP

885   values observed in our study and that of Briggs et al. (2018) and Alkire et al. (2012) highlight a

886   number of methodological limitations that could depress NPP estimates.

887   One possibility, which has been discussed at length by various authors (Gieskes et al.,

888   1979; Fogg and Calvario-Martinez, 1989; Marra, 2009), is that bottle containment effects limit

889   accurate estimates of ^{14}C uptake. This effect would have caused underestimates of ^{14}C-NPP

890   during both drifter surveys, relative to CbPM-NPP and NCP$_{O2/Ar}$, which do not require discrete

891   sample incubations. In addition, during the last ^{14}C-uptake experiment of drifter survey 2, the

892   incubator warmed (as the ship passed through warm SST water used to cool the tanks),

893   potentially creating heat stress on phytoplankton and depressing ^{14}C-NPP values.

894   A number of factors may also influence CbPM-based NPP estimates. While the model

895   applies a satellite-based relationship between [Chl-a]/[C$_{ph}$] and daily mixed layer irradiance (E$_g$)

896   to calculate growth rate, these E$_g$ values may not fully parametrize phytoplankton physiology for

897   mixed assemblages in the ocean (Westberry et al., 2008). Indeed, phytoplankton

898   photophysiology varies with other environmental conditions and phytoplankton composition

899   (Cloern et al., 1995; Geider et al., 1998; MacIntyre et al., 2002; Westberry et al., 2008). In

900   addition, the CbPM does not allow calculated growth rates to exceed 2 d$_{-1}$, which may not apply

901   to all ocean environments (Graff et al., 2016). These uncertainties could potentially impact the

902   applicability of the CbPM parameters to the specific ocean conditions at drifter sites 1 and 2. In

903 addition, a vertical mixing correction for ac-s and backscatter-derived [Chl-a] and [C_{ph}],

904 respectively, not feasible in the present data set, may improve CbPM-based estimates of NPP.

905

906 **5 Conclusions**

907

908   In the current study, biological oxygen saturation (ΔO_2/Ar) and optically-derived

909 particulate organic carbon (POC) were measured continuously and simultaneously during two

910 Lagrangian drifter deployments. This dual measurement approach facilitated direct comparison

911 of O_2/Ar and POC-derived measures of gross primary productivity (GPP), community respiration

912 (CR), and net community production (NCP), from a mesotrophic upwelling-influenced system

913 and a more oligotrophic system further offshore. As hypothesized, the results show that O_2 and

914 POC-based measures of GPP and NCP diverge in mid-to-high productivity phytoplankton

915 communities, where daily fluctuations in ΔO_2/Ar are decoupled from POC cycling. Interestingly,

916 oxygen-based GPP and CR also exceeded POC-based GPP and CR rates at the lower

917 productivity site, though we found that net changes in POC scaled with ΔO_2/Ar-based

918 productivity estimates, suggesting a tighter coupling between O_2 and POC cycles.

919   These findings are generally consistent with current understanding of productivity

920 dynamics and mixed layer POC cycling in these two coastal Pacific environments, and

921 complement only one prior comparison of daily GPP and NCP estimates from simultaneous,

922 autonomous measurements of c_P and O_2 in the North Atlantic mixed layer (Alkire et al., 2012;

923 Briggs et al., 2018). Importantly, however, our results differ from earlier studies by providing

924 two examples of significant disagreement between GPP$_{O2/Ar}$ and GPP$_{POC}$, and CR$_{O2/Ar}$ and

925 CR$_{POC}$, likely resulting from sub-daily variations in particle export, net DOC production, and

926 bacterial growth over respiration. In such cases, assuming constant daily respiration rates by

927 extrapolating nighttime rates of change may pose challenges for comparing ΔO_2/Ar and POC-

928 based GPP and CR. We have further shown that for upwelling regions like drifter site 1, it is

929 important to account for vertical mixing of sub-surface waters into the mixed layer, and its effect

930 on not only NCP$_{O2/Ar}$ calculations (Izett et al., 2018), but also on NCP$_{POC}$ estimates through

931 dilution of the surface POC signature. Our study thus illustrates an application of the vertical

932 mixing coefficient, k_{mix}, derived from [N_2O] profiles to more accurately estimate net changes in

933 POC and nutrient concentration in such environments.

934   Moving forward, the disparity between POC and O_2-based NCP estimates offers an
935   opportunity to continuously track cumulative POC losses in the mixed layer using autonomous
936   ship-board or in situ sensors. As it is labor intensive to measure POC export on short time scales
937   with sediment traps and the ^{234}Th-^{238}U disequilibrium method (Buesseler et al., 2006; Savoye et
938   al., 2006), simultaneous underway measurements of dissolved O_2, particulate beam attenuation
939   and CDOM absorption and spectral slope over a range of wavelengths <400 nm (Del Vecchio
940   and Blough, 2004; Grunert et al., 2018) may provide a valuable, first-order approximation of
941   POC partitioning among living phytoplankton biomass, particle export and dissolved organic
942   carbon (DOC) in the surface ocean on short time scales. At drifter site 1, for example, taking an
943   upper bound of 40% of NCP as DOC production (close to the fraction estimated Alkire et al.
944   (2012) during the North Atlantic spring bloom) yields a 3-day average DOC flux of 55 mmol C
945   m_{-2} d_{-1} and residual export flux of 76 mmol C m_{-2} d_{-1}. Being able to estimate such quantities with
946   this approach is especially important in the California coastal upwelling regime and other similar
947   ecosystems with high NCP and significant potential for carbon transfer to higher trophic levels.
948   For future work, we recommend a number of approaches to facilitate estimation of POC
949   export from coupled O_2, POC, and DOC dynamics. First, it will be valuable to constrain particle
950   size, and partitioning of POC into detrital and living (phytoplankton and heterotrophic bacteria)
951   components to properly assess the size range captured by optically-derived POC and C_{ph}
952   measurements. Second, independent estimates of POC export and DOC concentrations during
953   each drifter deployment could validate POC export fluxes derived from coupled O_2 and POC
954   measurements. Relatedly, depth-resolved backscatter profiles (Briggs et al., 2013, 2018) could be
955   used as another autonomous approach to calculating export fluxes, as an independent check on
956   surface-based estimates. Going forward, there is significant future potential to exploit coupled O_2
957   and c_p measurements on autonomous platforms, including various ocean moorings (e.g., the
958   Optical Dynamics Experiment, the Biowatt II program, and the Bermuda Testbed Mooring
959   program), and biogeochemical floats and gliders to resolve opportunistic, high-resolution POC
960   export time series (Stramska and Dickey, 1992; Kinkade et al., 1999; Dickey and Chang, 2002).
961   Deployment of such autonomous measurement systems across a range of oceanic regions will
962   help to constrain POC and productivity dynamics on global scales.
963
964   **Data availability**

965

Discrete and underway optical measurements may be accessed at

https://github.com/srosengard/rosengard-tortell-oc2017.git

Author contributions

Sarah Rosengard, Philippe Tortell, and Nina Schuback collected the data in the field. Robert Izett
processed the CTD cast data and measured nitrous oxide concentrations in discrete samples.
Sarah Rosengard wrote the manuscript with significant input from the co-authors.

Competing interests

The authors declare that they have no conflict of interest.

Acknowledgements

Special thanks to Jessie Gwinn, Ross McCulloch, Chen Zeng, Melissa Beaulac, Chris Payne and
Maureen Soon for assistance in field collection and analysis of samples, and to two anonymous
reviewers for insightful suggestions on earlier versions of this manuscript. This project was
funded by the Natural Sciences and Engineering Research Council of Canada (NSERC), and by
the US National Science Foundation (NSF project number 1436344).

References

Alkire, M. B., D'Asaro, E., Lee, C., Jane Perry, M., Gray, A., Cetinić, I., Briggs, N., Rehm, E.,
Kallin, E., Kaiser, J. and González-Posada, A.: Estimates of net community production and
export using high-resolution, Lagrangian measurements of O2, NO3−, and POC through the
evolution of a spring diatom bloom in the North Atlantic, Deep Sea Res. Part I Oceanogr. Res.
Pap., 64, 157–174, doi:10.1016/j.dsr.2012.01.012, 2012.

Anderson, L. A., and Sarmiento, J. L.: Redfield ratios of remineralization determined by nutrient
data analysis, Global biogeochem. cycles, 8(1), 65-80, 1994.

996   Barnes, M., and Antoine, D.: Proxies of community production derived from the diel variability

997   of particulate attenuation and backscattering coefficients in the northwest Mediterranean

998   Sea, Limnol. Oceanogr., 59(6), 2133-2149, 2014.

999   Behrenfeld, M. J., Boss, E., Siegel, D. A. and Shea, D. M.: Carbon-based ocean productivity and

1000   phytoplankton physiology from space, Global Biogeochem. Cycles, 19(1), 2005.

1001   Bif, M. B. and Hansell, D. A.: Seasonality of dissolved organic carbon in the upper Northeast

1002   Pacific Ocean, Global Biogeochem. Cycles, 2019.

1003   Bif, M. B., Hansell, D. A. and Popendorf, K. J.: Controls on the fate of dissolved organic carbon

1004   under contrasting upwelling conditions, Front. Mar. Sci., 5, 463, 2018.

1005   Boss, E., Twardowski, M. S. and Herring, S.: Shape of the particulate beam attenuation spectrum

1006   and its inversion to obtain the shape of the particulate size distribution, Appl. Opt., 40(27), 4885–

1007   4893, 2001.

1008   de Boyer Montégut, C., Madec, G., Fischer, A. S., Lazar, A. and Iudicone, D.: Mixed layer depth

1009   over the global ocean: An examination of profile data and a profile-based climatology, J.

1010   Geophys. Res., 109(C12), C12003, doi:10.1029/2004JC002378, 2004.

1011   Briggs, N., Guðmundsson, K., Cetinić, I., D'Asaro, E., Rehm, E., Lee, C. and Perry, M. J.: A

1012   multi-method autonomous assessment of primary productivity and export efficiency in the

1013   springtime North Atlantic, Biogeosciences, 15(14), 4515–4532, 2018.

1014   Briggs, N. T., Slade, W. H., Boss, E. and Perry, M. J.: Method for estimating mean particle size

1015   from high-frequency fluctuations in beam attenuation or scattering measurements, Appl. Opt.,

1016   52(27), 6710–6725, 2013.

1017   Brunet, C. and Lizon, F.: Tidal and diel periodicities of size-fractionated phytoplankton pigment

1018   signatures at an offshore station in the southeastern English Channel, Estuar. Coast. Shelf Sci.,

1019   56(3–4), 833–843, 2003.

1020   Brzezinski, M., Villareal, T. and Lipschultz, F.: Silica production and the contribution of diatoms

1021   to new and primary production in the central North Pacific, Mar. Ecol. Prog. Ser., 167, 89–104,

1022   doi:10.3354/meps167089, 1998.

1023   Brzezinski, M. A.: The Si:C:N ratio of marine diatoms: Interspecific variability and the effect of

1024   some environmental variables, J. Phycol., 21(3), 347–357, doi:10.1111/j.0022-

1025   3646.1985.00347.x, 2004.

1026   Brzezinski, M. A., Krause, J. W., Bundy, R. M., Barbeau, K. A., Franks, P., Goericke, R.,

Landry, M. R. and Stukel, M. R.: Enhanced silica ballasting from iron stress sustains carbon export in a frontal zone within the California Current, J. Geophys. Res. Ocean., 120(7), 4654–4669, 2015.

Buesseler, K. O.: The decoupling of production and particulate export in the surface ocean, Global Biogeochem. Cycles, 12(2), 297–310, 1998.

Buesseler, K. O., Benitez-Nelson, C. R., Moran, S. B., Burd, A., Charette, M., Cochran, J. K., Coppola, L., Fisher, N. S., Fowler, S. W. and Gardner, W. D.: An assessment of particulate organic carbon to thorium-234 ratios in the ocean and their impact on the application of 234Th as a POC flux proxy, Mar. Chem., 100(3–4), 213–233, 2006.

Burt, W. J. and Tortell, P. D.: Observations of Zooplankton Diel Vertical Migration From High-Resolution Surface Ocean Optical Measurements, Geophys. Res. Lett., 45(24), 13–396, 2018.

Burt, W. J., Westberry, T. K., Behrenfeld, M. J., Zeng, C., Izett, R. W. and Tortell, P. D.: Carbon: Chlorophyll Ratios and Net Primary Productivity of Subarctic Pacific Surface Waters Derived From Autonomous Shipboard Sensors, Global Biogeochem. Cycles, 32(2), 267–288, doi:10.1002/2017GB005783, 2018.

Capelle, D. W., Dacey, J. W. and Tortell, P. D.: An automated, high through-put method for accurate and precise measurements of dissolved nitrous-oxide and methane concentrations in natural waters, Limnol. Oceanogr. Methods, 13(7), 345–355, 2015.

Cassar, N., Barnett, B. A., Bender, M. L., Kaiser, J., Hamme, R. C. and Tilbrook, B.: Continuous high-frequency dissolved O2/Ar measurements by equilibrator inlet mass spectrometry, Anal. Chem., 81(5), 1855–1864, 2009.

Cassar, N., Nevison, C. D. and Manizza, M.: Correcting oceanic O2/Ar-net community production estimates for vertical mixing using N2O observations, Geophys. Res. Lett., 41(24), 8961–8970, 2014.

Church, M. J., Ducklow, H. W., and Karl, D. M.: Light dependence of [3H] leucine incorporation in the oligotrophic North Pacific Ocean, Appl. Environ. Microbiol., 70(7), 4079-4087, 2004.

Claustre, H., Morel, A., Babin, M., Cailliau, C., Marie, D., Marty, J., Tailliez, D. and Vaulot, D.: Variability in particle attenuation and chlorophyll fluorescence in the tropical Pacific: Scales, patterns, and biogeochemical implications, J. Geophys. Res. Ocean., 104(C2), 3401–3422, 1999.

Claustre, H., Huot, Y., Obernosterer, I., Gentili, B., Tailliez, D. and Lewis, M.: Gross community

production and metabolic balance in the South Pacific Gyre, using a non intrusive bio-optical method, Biogeosciences, 5, 463-474, 2008.

Cloern, J. E., Grenz, C. and Vidergar-Lucas, L.: An empirical model of the phytoplankton chlorophyll: carbon ratio-the conversion factor between productivity and growth rate, Limnol. Oceanogr., 40(7), 1313–1321, 1995.

Dagg, M. J., Vidal, J., Whitledge, T. E., Iverson, R. L. and Goering, J. J.: The feeding, respiration, and excretion of zooplankton in the Bering Sea during a spring bloom, Deep Sea Res. Part A. Oceanogr. Res. Pap., 29(1), 45–63, 1982.

Dall'Olmo, G., Boss, E., Behrenfeld, M. J., Westberry, T. K., Courties, C., Prieur, L., Pujo-Pay, M., Hardman-Mountford, N. and Moutin, T.: Inferring phytoplankton carbon and eco-physiological rates from diel cycles of spectral particulate beam-attenuation coefficient, Biogeosciences, 8(11), 3423–3439, 2011.

Daneri, G., Lizárraga, L., Montero, P., González, H. E., and Tapia, F. J.: Wind forcing and short-term variability of phytoplankton and heterotrophic bacterioplankton in the coastal zone of the Concepción upwelling system (Central Chile), Prog. Oceanogr., 92, 92-96, 2012.

Del Vecchio, R., and Blough, N. V.: Spatial and seasonal distribution of chromophoric dissolved organic matter and dissolved organic carbon in the Middle Atlantic Bight, Mar. Chem., 89(1-4), 169-187, 2004.

Dickey, T. D. and Chang, G. C.: Recent advances and future visions: temporal variability of optical and bio-optical properties of the ocean, Oceanogr. DC-OCEANOGRAPHY Soc., 14(3), 15–29, 2002.

Dugenne, M., Thyssen, M., Nerini, D., Mante, C., Poggiale, J.-C., Garcia, N., Garcia, F. and Grégori, G. J.: Consequence of a sudden wind event on the dynamics of a coastal phytoplankton community: an insight into specific population growth rates using a single cell high frequency approach, Front. Microbiol., 5, 485, 2014.

Durand, M. D., and Olson, R. J.: Diel patterns in optical properties of the chlorophyte Nannochloris sp.: Relating individual-cell to bulk measurements, Limnol. Oceanogr., 43(6), 1107-1118, 1998.

Fernández-Urruzola, I., Osma, N., Packard, T. T., Gómez, M., and Postel, L.: Distribution of zooplankton biomass and potential metabolic activities across the northern Benguela upwelling system, J Marine Syst, 140, 138-149, 2014.

1089 Ferrón, S., Wilson, S. T., Martínez-García, S., Quay, P. D., and Karl, D. M.: Metabolic balance

1090 in the mixed layer of the oligotrophic North Pacific Ocean from diel changes in O2/Ar saturation

1091 ratios, Geophys. Res. Lett., 42(9), 3421-3430, 2015.

1092 Fogg, G. E. and Calvario-Martinez, O.: Effects of bottle size in determinations of primary

1093 productivity by phytoplankton, Hydrobiologia, 173(2), 89–94, doi:10.1007/BF00015518, 1989.

1094 Fowler, S. W. and Knauer, G. A.: Role of large particles in the transport of elements and organic

1095 compounds through the oceanic water column, Prog. Oceanogr., 16(3), 147–194,

1096 doi:10.1016/0079-6611(86)90032-7, 1986.

1097 Fuhrman, J. A., Eppley, R. W., Hagström, Å., and Azam, F.: Diel variations in bacterioplankton,

1098 phytoplankton, and related parameters in the Southern California Bight, Mar. Ecol. Prog. Ser, 27,

1099 9-20, 1985.

1100 Garcia, H. E. and Gordon, L. I.: Oxygen solubility in seawater: Better fitting equations, Limnol.

1101 Oceanogr., 37(6), 1307–1312, 1992.

1102 Gardner, W. D., Walsh, I. D. and Richardson, M. J.: Biophysical forcing of particle production

1103 and distribution during a spring bloom in the North Atlantic, Deep Sea Res. Part II Top. Stud.

1104 Oceanogr., 40(1–2), 171–195, 1993.

1105 Geider, R. J., Maclntyre, H. L. and Kana, T. M.: A dynamic regulatory model of phytoplanktonic

1106 acclimation to light, nutrients, and temperature, Limnol. Oceanogr., 43(4), 679–694, 1998.

1107 Gernez, P., Antoine, D. and Huot, Y.: Diel cycles of the particulate beam attenuation coefficient

1108 under varying trophic conditions in the northwestern Mediterranean Sea: Observations and

1109 modeling, Limnol. Oceanogr., 56(1), 17–36, 2011.

1110 Gieskes, W. W. C., Kraay, G. W. and Baars, M. A.: Current 14C methods for measuring primary

1111 production: Gross underestimates in oceanic waters, Netherlands J. Sea Res., 13(1), 58–78,

1112 doi:10.1016/0077-7579(79)90033-4, 1979.

1113 Graff, J. R., Westberry, T. K., Milligan, A. J., Brown, M. B., Dall'Olmo, G., Dongen-Vogels, V.

1114 van, Reifel, K. M. and Behrenfeld, M. J.: Analytical phytoplankton carbon measurements

1115 spanning diverse ecosystems, Deep Sea Res. Part I Oceanogr. Res. Pap., 102, 16–25,

1116 doi:10.1016/J.DSR.2015.04.006, 2015.

1117 Graff, J. R., Westberry, T. K., Milligan, A. J., Brown, M. B., Olmo, G. D., Reifel, K. M. and

1118 Behrenfeld, M. J.: Photoacclimation of natural phytoplankton communities, Mar. Ecol. Prog.

1119 Ser., 542, 51–62, 2016.

1120   Grunert, B. K., Mouw, C. B., and Ciochetto, A. B.: Characterizing CDOM spectral variability

1121   across diverse regions and spectral ranges, Global Biogeochem. Cycles, 32(1), 57-77, 2018.

1122   Guidi, L., Jackson, G. A., Stemmann, L., Carlos Miquel, J., Picheral, M. and Gorsky, G.:

1123   Author's personal copy Relationship between particle size distribution and flux in the

1124   mesopelagic zone, , doi:10.1016/j.dsr.2008.05.014, 2008.

1125   Guidi, L., Stemmann, L., Jackson, G. A., Ibanez, F., Claustre, H., Legendre, L., Picheral, M. and

1126   Gorskya, G.: Effects of phytoplankton community on production, size, and export of large

1127   aggregates: A world-ocean analysis, Limnol. Oceanogr., 54(6), 1951–1963, 2009.

1128   Hamme, R. C., Cassar, N., Lance, V. P., Vaillancourt, R. D., Bender, M. L., Strutton, P. G.,

1129   Moore, T. S., DeGrandpre, M. D., Sabine, C. L. and Ho, D. T.: Dissolved O_2/Ar and other

1130   methods reveal rapid changes in productivity during a Lagrangian experiment in the Southern

1131   Ocean, J. Geophys. Res. Ocean., 117(C4), 2012.

1132   Hansell, D. A. and Carlson, C. A.: Net community production of dissolved organic carbon,

1133   Global Biogeochem. Cycles, 12(3), 443–453, 1998.

1134   Hedges, J. I., Baldock, J. A., Gélinas, Y., Lee, C., Peterson, M. L., and Wakeham, S. G.: The

1135   biochemical and elemental compositions of marine plankton: A NMR perspective, Mar.

1136   Chem., 78(1), 47-63, 2002.

1137   Henson, S. A., Sanders, R. and Madsen, E.: Global patterns in efficiency of particulate organic

1138   carbon export and transfer to the deep ocean, Global Biogeochem. Cycles, 26(1), 2012.

1139   Hickey, B. M., Pietrafesa, L. J., Jay, D. A. and Boicourt, W. C.: The Columbia River plume

1140   study: Subtidal variability in the velocity and salinity fields, J. Geophys. Res. Ocean., 103(C5),

1141   10339–10368, 1998.

1142   Hirata, T., Hardman-Mountford, N. J., Brewin, R. J. W., Aiken, J., Barlow, R., Suzuki, K., Isada,

1143   T., Howell, E., Hashioka, T. and Noguchi-Aita, M.: Synoptic relationships between surface

1144   Chlorophyll-a and diagnostic pigments specific to phytoplankton functional types,

1145   Biogeosciences, 8(2), 311–327, 2011.

1146   Hopkinson, B. M., and Barbeau, K.A.: Organic and redox speciation of iron in the eastern

1147   tropical North Pacific suboxic zone, Mar. Chem., 106(1-2), 2-17, 2007.

1148   Hoppe, C. J. M., Schuback, N., Semeniuk, D. M., Maldonado, M. T. and Rost, B.: Functional

1149   Redundancy Facilitates Resilience of Subarctic Phytoplankton Assemblages toward Ocean

1150   Acidification and High Irradiance , Front. Mar. Sci. , 4, 229 [online] Available from:

https://www.frontiersin.org/article/10.3389/fmars.2017.00229, 2017.

Izett, R. W., Manning, C. C., Hamme, R. C. and Tortell, P. D.: Refined estimates of net community production in the Subarctic Northeast Pacific derived from $\Delta O_2/Ar$ measurements with N2O-based corrections for vertical mixing, Global Biogeochem. Cycles, 32(3), 326–350, 2018.

Jin, X., Najjar, R. G., Louanchi, F. and Doney, S. C.: A modeling study of the seasonal oxygen budget of the global ocean, J. Geophys. Res. Ocean., 112(C5), 2007.

Kaiser, J., Reuer, M. K., Barnett, B. and Bender, M. L.: Marine productivity estimates from continuous O2/Ar ratio measurements by membrane inlet mass spectrometry, Geophys. Res. Lett., 32(19), 2005.

Karl, D. M., Hebel, D. V., Björkman, K., and Letelier, R. M.: The role of dissolved organic matter release in the productivity of the oligotrophic North Pacific Ocean, Limnol. Oceanogr., 43(6), 1270-1286, 1998.

Keeling, R. F. and Shertz, S. R.: Seasonal and interannual variations in atmospheric oxygen and implications for the global carbon cycle, Nature, 358(6389), 723, 1992.

Kheireddine, M. and Antoine, D.: Diel variability of the beam attenuation and backscattering coefficients in the northwestern Mediterranean Sea (BOUSSOLE site), J. Geophys. Res. Ocean., 119(8), 5465–5482, 2014.

Kinkade, C. S., Marra, J., Dickey, T. D., Langdon, C., Sigurdson, D. E. and Weller, R.: Diel bio-optical variability observed from moored sensors in the Arabian Sea, Deep sea Res. Part II Top. Stud. Oceanogr., 46(8–9), 1813–1831, 1999.

Kostadinov, T. S., Siegel, D. A. and Maritorena, S.: Retrieval of the particle size distribution from satellite ocean color observations, J. Geophys. Res., 114(C9), C09015, doi:10.1029/2009JC005303, 2009.

Kuipers, B., van Noort, G. J., Vosjan, J., and Herndl, G. J.: Diel periodicity of bacterioplankton in the euphotic zone of the subtropical Atlantic Ocean, Mar. Ecol. Prog. Ser., 201, 13-25, 2000.

Laws, E. A.: Photosynthetic quotients, new production and net community production in the open ocean, Deep Sea Res. Part A. Oceanogr. Res. Pap., 38(1), 143–167, 1991.

Lide, D. R.: Physical and optical properties of minerals, CRC Handb. Chem. Phys., 4–130, 1997.

Lochte, K., Ducklow, H. W., Fasham, M. J. R. and Stienen, C.: Plankton succession and carbon cycling at 47 N 20 W during the JGOFS North Atlantic Bloom Experiment, Deep Sea Res. Part

1182 II Top. Stud. Oceanogr., 40(1–2), 91–114, 1993.

1183 Loisel, H., Nicolas, J.-M., Sciandra, A., Stramski, D. and Poteau, A.: Spectral dependency of

1184 optical backscattering by marine particles from satellite remote sensing of the global ocean, J.

1185 Geophys. Res., 111(C9), C09024, doi:10.1029/2005JC003367, 2006.

1186 Lønborg, C., Martínez-García, S., Teira, E., and Álvarez-Salgado, X. A.: Bacterial carbon

1187 demand and growth efficiency in a coastal upwelling system, Aquat. Microb. Ecol., 63(2), 183-

1188 191, 2011.

1189 MacIntyre, H. L., Kana, T. M., Anning, T. and Geider, R. J.: Photoacclimation of irradiance

1190 response curves and photosynthetic pigments in microalgae and cyanobacteria, J. Phycol., 38(1),

1191 17–38, doi:10.1046/j.1529-8817.2002.00094.x, 2002.

1192 Manning, C. C., Stanley, R. H. R., Nicholson, D. P., Smith, J. M., Pennington, J. T., Fewings, M.

1193 R., Squibb, M. E. and Chavez, F. P.: Impact of recently upwelled water on productivity

1194 investigated using in situ and incubation-based methods in Monterey Bay, J. Geophys. Res.

1195 Ocean., 122(3), 1901–1926, 2017.

1196 Marra, J.: Approaches to the measurement of plankton production, Phytoplankt. Product. Carbon

1197 Assim. Mar. Freshw. Ecosyst., 78–108, 2002.

1198 Marra, J.: Net and gross productivity: weighing in with 14C, Aquat. Microb. Ecol., 56(2–3),

1199 123–131, doi:10.3354/ame01306, 2009.

1200 Morel, A., Huot, Y., Gentili, B., Werdell, P. J., Hooker, S. B. and Franz, B. A.: Examining the

1201 consistency of products derived from various ocean color sensors in open ocean (Case 1) waters

1202 in the perspective of a multi-sensor approach, Remote Sens. Environ., 111(1), 69–88, 2007.

1203 Murphy, J. and Riley, J. P.: A modified single solution method for the determination of

1204 phosphate in natural waters, Anal. Chim. Acta, 27, 31–36, 1962.

1205 Needham, D. M. and Fuhrman, J. A.: Pronounced daily succession of phytoplankton, archaea

1206 and bacteria following a spring bloom, Nat. Microbiol., 1(4), 16005, 2016.

1207 Nicholson, D. P., Wilson, S. T., Doney, S. C. and Karl, D. M.: Quantifying subtropical North

1208 Pacific gyre mixed layer primary productivity from Seaglider observations of diel oxygen cycles,

1209 Geophys. Res. Lett., 42(10), 4032–4039, 2015.

1210 Oubelkheir, K., and Sciandra, A.: Diel variations in particle stocks in the oligotrophic waters of

1211 the Ionian Sea (Mediterranean), J. Marine Syst., 74(1-2), 364-371, 2008.

1212 Raymond, P. A., Zappa, C. J., Butman, D., Bott, T. L., Potter, J., Mulholland, P., Laursen, A. E.,

1213   McDowell, W. H. and Newbold, D.: Scaling the gas transfer velocity and hydraulic geometry in

1214   streams and small rivers, Limnol. Oceanogr. Fluids Environ., 2(1), 41–53, 2012.

1215   Reuer, M. K., Barnett, B. A., Bender, M. L., Falkowski, P. G. and Hendricks, M. B.: New

1216   estimates of Southern Ocean biological production rates from O2/Ar ratios and the triple isotope

1217   composition of O2, Deep Sea Res. Part I Oceanogr. Res. Pap., 54(6), 951–974, 2007.

1218   Ribalet, F., Swalwell, J., Clayton, S., Jiménez, V., Sudek, S., Lin, Y., Johnson, Z. I., Worden, A.

1219   Z. and Armbrust, E. V.: Light-driven synchrony of Prochlorococcus growth and mortality in the

1220   subtropical Pacific gyre, Proc. Natl. Acad. Sci., 112(26), 8008–8012, 2015.

1221   Riley, J. P.: Grasshoff, K. [Ed.] 1976. Methods of seawater analysis. Verlag Chemie, Weinheim

1222   and New York, xv+ 317 p. $43.60., 1977.

1223   Robinson, C., and Williams, P. J. L. B.: Plankton net community production and dark

1224   respiration in the Arabian Sea during September 1994, Deep Sea Res. Part II Top. Stud.

1225   Oceanogr., 46(3-4), 745-765, 1999.

1226   Robinson, C., Archer, S. D., and Williams, P. J. L. B.: Microbial dynamics in coastal waters of

1227   East Antarctica: plankton production and respiration, Mar. Ecol. Prog. Ser., 180, 23-36, 1999.

1228   Robinson, C., Serret, P., Tilstone, G., Teira, E., Zubkov, M. V., Rees, A. P., and Woodward, E.

1229   M. S.: Plankton respiration in the eastern Atlantic Ocean, Deep Sea Res. Part I Oceanogr. Res.

1230   Pap., 49(5), 787-813, 2002.

1231   Roesler, C. S. and Barnard, A. H.: Optical proxy for phytoplankton biomass in the absence of

1232   photophysiology: Rethinking the absorption line height, Methods Oceanogr., 7, 79–94, 2013.

1233   Savoye, N., Benitez-Nelson, C., Burd, A. B., Cochran, J. K., Charette, M., Buesseler, K. O.,

1234   Jackson, G. A., Roy-Barman, M., Schmidt, S. and Elskens, M.: 234Th sorption and export

1235   models in the water column: a review, Mar. Chem., 100(3–4), 234–249, 2006.

1236   Schuback, N., and Tortell, P. D.: Diurnal regulation of photosynthetic light absorption, electron

1237   transport and carbon fixation in two contrasting oceanic environments, Biogeosciences, 16(7),

1238   1381-1399, 2019.

1239   Schuback, N., Flecken, M., Maldonado, M. T. and Tortell, P. D.: Diurnal variation in the

1240   coupling of photosynthetic electron transport and carbon fixation in iron-limited phytoplankton

1241   in the NE subarctic Pacific, Biogeosciences, 13, 1019–1035, doi:10.5194/bg-13-1019-2016,

1242   2016.

1243   Siegel, D. A., Dickey, T. D., Washburn, L., Hamilton, M. K. and Mitchell, B. G.: Optical

1244 determination of particulate abundance and production variations in the oligotrophic ocean, Deep

1245 Sea Res. Part A. Oceanogr. Res. Pap., 36(2), 211–222, 1989.

1246 Stanley, R. H. R., Kirkpatrick, J. B., Cassar, N., Barnett, B. A. and Bender, M. L.: Net

1247 community production and gross primary production rates in the western equatorial Pacific,

1248 Global Biogeochem. Cycles, 24(4), 2010.

1249 Stramska, M. and Dickey, T. D.: Short-term variations of the bio-optical properties of the ocean

1250 in response to cloud-induced irradiance fluctuations, J. Geophys. Res. Ocean., 97(C4), 5713–

1251 5721, 1992.

1252 Stramska, M. and Dickey, T. D.: Modeling phytoplankton dynamics in the northeast Atlantic

1253 during the initiation of the spring bloom, J. Geophys. Res. Ocean., 99(C5), 10241–10253, 1994.

1254 Stramska, M., Stramski, D., Hapter, R., Kaczmarek, S. and Ston´, J. S.: Bio-optical relationships

1255 and ocean color algorithms for the north polar region of the Atlantic, J. Geophys. Res, 108(C5),

1256 3143, doi:10.1029/2001JC001195, 2003.

1257 Stramski, D. and Kiefer, D. A.: Light scattering by microorganisms in the open ocean, Prog.

1258 Oceanogr., 28(4), 343–383, doi:10.1016/0079-6611(91)90032-H, 1991.

1259 Stramski, D. and Reynolds, R. A.: Diel variations in the optical properties of a marine diatom,

1260 Limnol. Oceanogr., 38(7), 1347–1364, 1993.

1261 Stukel, M. R., Aluwihare, L. I., Barbeau, K. A., Chekalyuk, A. M., Goericke, R., Miller, A. J.,

1262 Ohman, M. D., Ruacho, A., Song, H. and Stephens, B. M.: Mesoscale ocean fronts enhance

1263 carbon export due to gravitational sinking and subduction, Proc. Natl. Acad. Sci., 114(6), 1252–

1264 1257, 2017.

1265 Sullivan, J. M., Twardowski, M. S., Donaghay, P. L. and Freeman, S. A.: Use of optical

1266 scattering to discriminate particle types in coastal waters, Appl. Opt., 44(9), 1667,

1267 doi:10.1364/AO.44.001667, 2005.

1268 Thomas, A. C. and Weatherbee, R. A.: Satellite-measured temporal variability of the Columbia

1269 River plume, Remote Sens. Environ., 100(2), 167–178, doi:10.1016/J.RSE.2005.10.018, 2006.

1270 Thomson, R. E., and Fine, I. V.: Estimating Mixed Layer Depth from Oceanic Profile Data, J.

1271 Atmos. Ocean. Technol., 20(2), 319–329, doi:10.1175/1520-

1272 0426(2003)020<0319:EMLDFO>2.0.CO;2, 2003.

1273 Thyssen, M., Grégori, G. J., Grisoni, J.-M., Pedrotti, M. L., Mousseau, L., Artigas, L. F., Marro,

1274 S., Garcia, N., Passafiume, O. and Denis, M. J.: Onset of the spring bloom in the northwestern

Mediterranean Sea: influence of environmental pulse events on the in situ hourly-scale dynamics of the phytoplankton community structure, Front. Microbiol., 5, 387, 2014.

Tortell, P. D.: Dissolved gas measurements in oceanic waters made by membrane inlet mass spectrometry, Limnol. Oceanogr. Methods, 3(1), 24–37, 2005.

Tortell, P. D., Guéguen, C., Long, M. C., Payne, C. D., Lee, P. and DiTullio, G. R.: Spatial variability and temporal dynamics of surface water pCO2, $\Delta O_2/Ar$ and dimethylsulfide in the Ross Sea, Antarctica, Deep Sea Res. Part I Oceanogr. Res. Pap., 58(3), 241–259, 2011.

Tortell, P. D., Asher, E. C., Ducklow, H. W., Goldman, J. A. L., Dacey, J. W. H., Grzymski, J. J., Young, J. N., Kranz, S. A., Bernard, K. S. and Morel, F. M. M.: Metabolic balance of coastal Antarctic waters revealed by autonomous pCO2 and $\Delta O_2/Ar$ measurements, Geophys. Res. Lett., 41(19), 6803–6810, 2014.

Turner, R. E., Qureshi, N., Rabalais, N. N., Dortch, Q., Justic, D., Shaw, R. F. and Cope, J.: Fluctuating silicate: nitrate ratios and coastal plankton food webs, Proc. Natl. Acad. Sci., 95(22), 13048–13051, 1998.

Twardowski, M. S., Boss, E., Macdonald, J. B., Pegau, W. S., Barnard, A. H. and Zaneveld, J. R. V.: A model for estimating bulk refractive index from the optical backscattering ratio and the implications for understanding particle composition in case I and case II waters, J. Geophys. Res. Ocean., 106(C7), 14129–14142, doi:10.1029/2000JC000404, 2001.

Waite, A. M., and Nodder, S. D.: The effect of in situ iron addition on the sinking rates and export flux of Southern Ocean diatoms, Deep Sea Res. Part II Top. Stud. Oceanogr., 48(11-12), 2635-2654, 2001.

Wanninkhof, R.: Relationship between wind speed and gas exchange over the ocean revisited, Limnol. Oceanogr. Methods, 12(6), 351–362, 2014.

Weiss, R. F. and Price, B. A.: Nitrous oxide solubility in water and seawater, Mar. Chem., 8(4), 347–359, 1980.

Westberry, T., Behrenfeld, M. J., Siegel, D. A. and Boss, E.: Carbon-based primary productivity modeling with vertically resolved photoacclimation, Global Biogeochem. Cycles, 22(2), 2008.

White, A. E., Barone, B., Letelier, R. M. and Karl, D. M.: Productivity diagnosed from the diel cycle of particulate carbon in the North Pacific Subtropical Gyre, Geophys. Res. Lett., 44(8), 3752–3760, 2017.

Wu, C.-J., Chiang, K.-P. and Liu, H.: Diel feeding pattern and prey selection of

1306   mesozooplankton on microplankton community, J. Exp. Mar. Bio. Ecol., 390(2), 134–142, 2010.

1307   Zeng, C., Rosengard, S. Z., Burt, W., Peña, M. A., Nemcek, N., Zeng, T., Arrigo, K. R. and

1308   Tortell, P. D.: Optically-derived estimates of phytoplankton size class and taxonomic group

1309   biomass in the Eastern Subarctic Pacific Ocean, Deep Sea Res. Part I Oceanogr. Res. Pap., 136,

1310   107–118, 2018.

1311

1312

1313 **Table 1**: Daily-integrated mixed layer net primary production (NPP) and net community

1314 production (NCP), including all components used to calculate NCP from $\Delta O_2/Ar$ or POC time

1315 series, as indicated: gross primary productivity (GPP), respiration (CR), vertical mixing (Mix),

1316 and gas exchange (J_{ex}). All units here are in mmol C m^{-2} d^{-1}. Note that CbPM is the Carbon-

1317 Based Production Model (Behrenfeld et al., 2005; Westberry et al., 2008; Graff et al., 2016)

1318 (Sect. 2.5).

1319

	Drifter 1:			Drifter 2:	
	Day 1	Day 2	Day 3	Day 1	Day 2
NPP (CbPM)	147 ± 61	137 ± 51	112 ± 40	22 ± 9	18 ± 7
NPP ($14C$)	150 ± 18	-	49 ± 8	12 ± 4	-
GPP ($\Delta O_2/Ar$)	284 ± 75	270 ± 178	358 ± 198	108 ± 101	219 ± 211
GPP (POC)	242 ± 51	106 ± 26	98 ± 35	41 ± 8	38 ± 7
R ($\Delta O_2/Ar$)	-73 ± 65	-150 ± 88	-172 ± 56	-83 ± 35	-186 ± 64
R (POC)	-77 ± 55	-147 ± 28	-104 ± 40	-44 ± 12	-36 ± 9
Mix (N_2O)	-70 ± 29	-16 ± 81	-19 ± 42	0	0
Mix (POC)	-67 ± 47	-12 ± 16	-20 ± 16	0	0
J_{ex} (daily)	-62 ± 11	-7 ± 4	-6 ± 3	12 ± 5	17 ± 7
NCP$_{O2/Ar}$	140 ± 45	104 ± 84	167 ± 52	-12 ± 44*	33 ± 20
NCP$_{POC}$	97 ± 49	-53 ± 24	-25 ± 31	-2 ± 3	1 ± 2

1320

1321 *Calculated using summed three-hour increments of NCP$_{O2/Ar}$ (refer to Table 2 and Sect. 2.6.3).

1322 All other NCP values reported here were computed using day/night linear regressions of [POC]

1323 and [O_2]$_{bio}$ against time (Sects. 2.6.1, 2.6.2).

1324

1325

1326

1327 **Table 2**: Comparisons of NCP calculated using four different time scales of integration: (rows 1-

1328 2) day/night linear regressions, (rows 3-4) summed linear regressions over 3-hour increments,

1329 (rows 5-6) the difference between two time points every 24 hours, and (rows 7-8) a single linear

1330 regression over the entire drifter period. Refer to Sect. 2.6.3 for further details. For every

1331 calculation approach, "Export + DOC" is the average difference between $NCP_{O2/Ar}$ and NCP_{POC}

1332 values $\pm$ 1 S.D. or $\pm$ the propagated error. All units here are in mmol C m^{-2} d^{-1}.

1333

	Drifter 1:			Mean ± S.D.	Export + DOC	Drifter 2:		Mean ± S.D.	Export + DOC
	Day 1	Day 2	Day 3			Day 1	Day 2		
$NCP_{O2/Ar}$	140 ± 45	104 ± 84	167 ± 52	137 ± 32		26 ± 18	33 ± 20	29 ± 5	
NCP_{POC}	97 ± 49	-53 ± 24	-25 ± 31	7 ± 80	131 ± 79	-2 ± 3	1 ± 2	-0.8 ± 3	30 ± 2.4
$NCP_{O2/Ar}$ **(3 hr)**	177 ± 121	129 ± 102	122 ± 157	143 ± 30		-12 ± 44	25 ± 75	6 ± 26	
NCP_{POC} **(3 hr)**	119 ± 66	-86 ± 64	53 ± 140	28 ± 105	115 ± 88	-8 ± 10	-6 ± 5	-7 ± 1	14 ± 25
$NCP_{O2/Ar}$ **(time points)**	180 ± 54	128 ± 84	78 ± 43	129 ± 51		-4 ± 13	26 ± 11	11 ± 21	
NCP_{POC} **(time points)**	99 ± 48	-73 ± 21	-14 ± 19	4 ± 87	125 ± 66	-6 ± 17	-2 ± 11	-4 ± 3	15 ± 18
$NCP_{O2/Ar}$ **(whole drifter trend)**				103 ± 56				13 ± 9	
NCP_{POC} **(drifter trend)**				-21 ± 28	123 ± 62			-4 ± 2	17 ± 9

1334
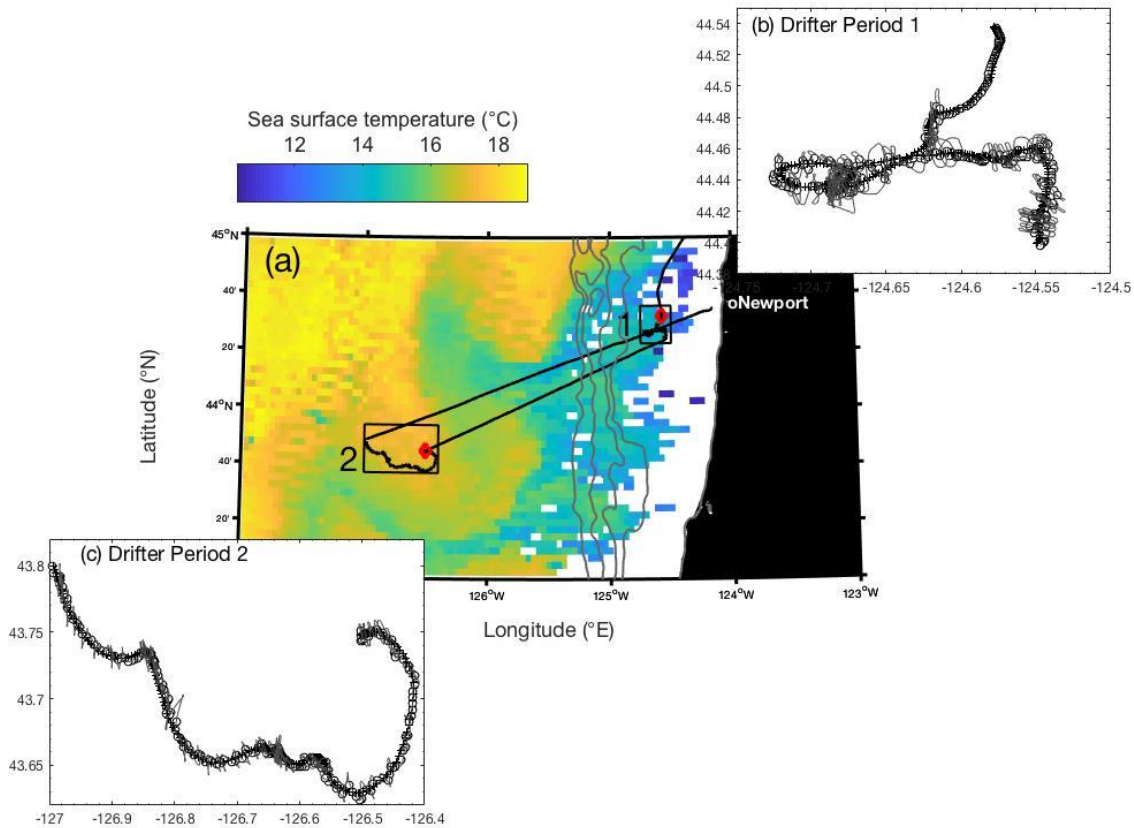
1335

1336

Figure 1: (a) Map of AQUA MODIS-derived 8-day composite sea surface temperature (11µm,

nighttime) from 21-28 August 2017, overlapping with the duration of both drifter deployments.

The two hollow boxes on the map denote location of drifter tracks, with the red diamonds

indicating the location of the initial release. Gray bathymetry contours represent 0, 500, 1000,

1500 and 2000 m depths. Panels (b and c) show a detailed view of the two drifter tracks (cross

symbol), with the ship's track shown in a light grey line and open circles denoting times when

the ship was <1.5 km away from the drifter position. Only measurements taken at these cross-

over locations were used for analysis.

1345
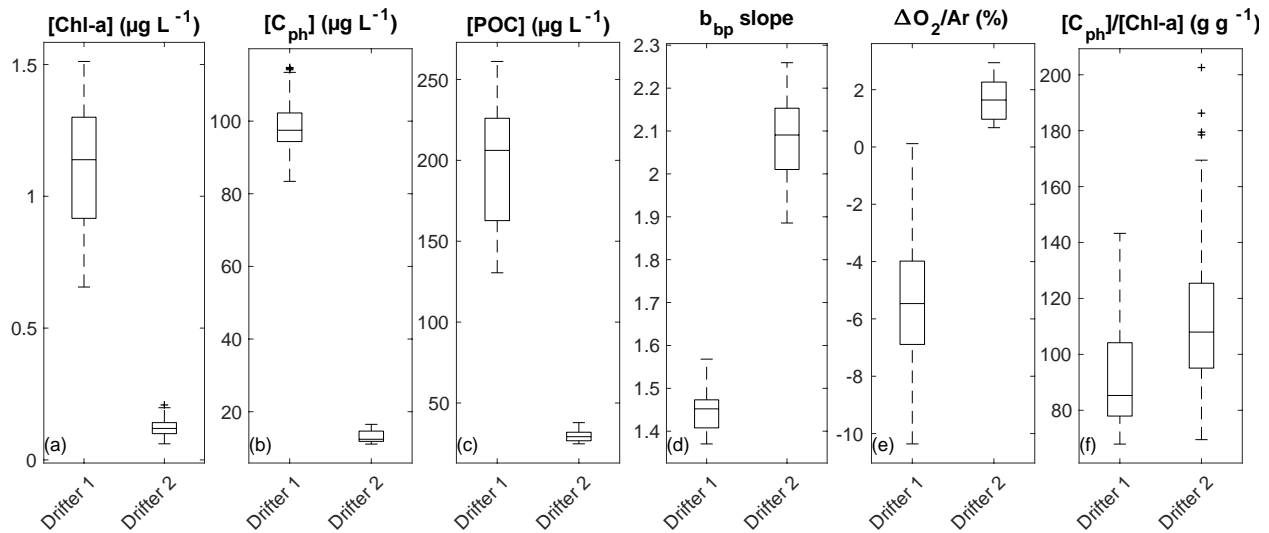
Figure 2: Comparison of average surface water properties between the two drifter deployments: (a) chlorophyll-a concentration (Chl-a), (b) phytoplankton carbon concentration (C_{ph}), (c) particulate organic carbon (POC) concentration, (d) the wavelength-dependent slope of particulate backscatter (b_{bp}), (e) biological oxygen saturation anomaly ($\Delta O_2/Ar$), and (f) the [C_{ph}]/[Chl-a] ratio. Boxes represent the median (center line) and 25 and 75 percentiles (box edges). Outliers are indicated as black "+" marks.
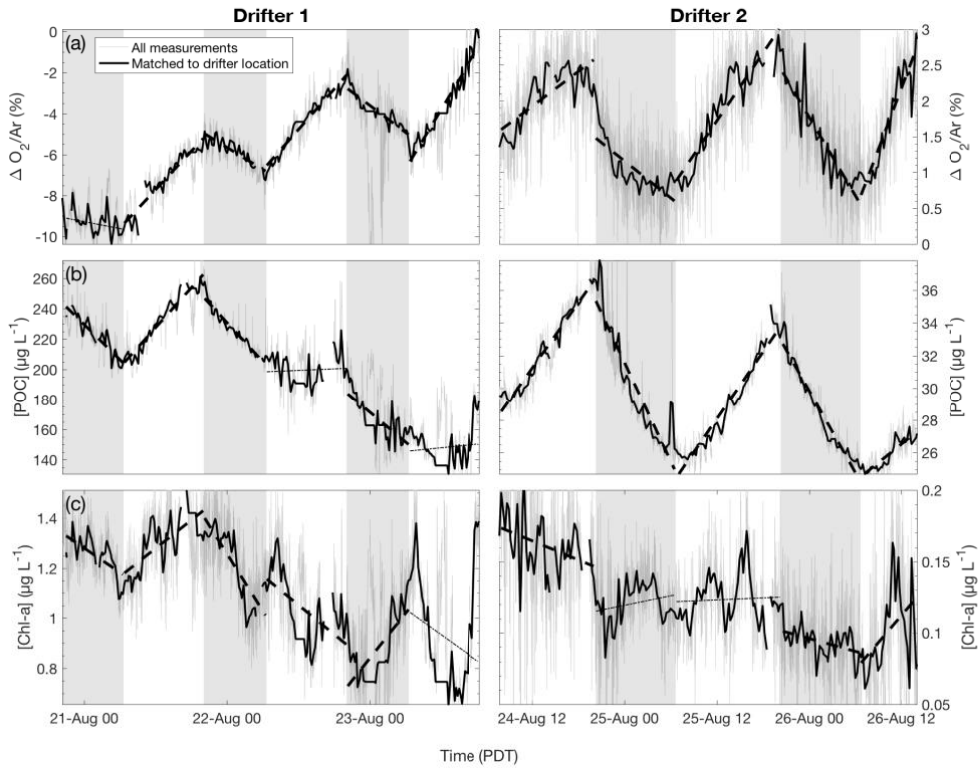
1355

1356 **Figure 3**: Time-series of (a) biological oxygen saturation (ΔO_2/Ar), (b) particulate organic

1357 carbon (POC) concentration, and (c) chlorophyll-a (Chl-a) concentration during the two drifter

1358 deployments (left and right panels, respectively). For each daytime (non-shaded) and nighttime

1359 (shaded) interval, the best fit linear regression line is plotted. Significant regressions ($p<0.05$) are

1360 plotted as thick dashed lines, while non-significant regressions ($p\geq0.05$) are plotted as thin dotted

1361 lines. Grey lines show all measurements while thicker black line shows observations collected

1362 when the ship was within 1.5 km of the drifter location.

1363
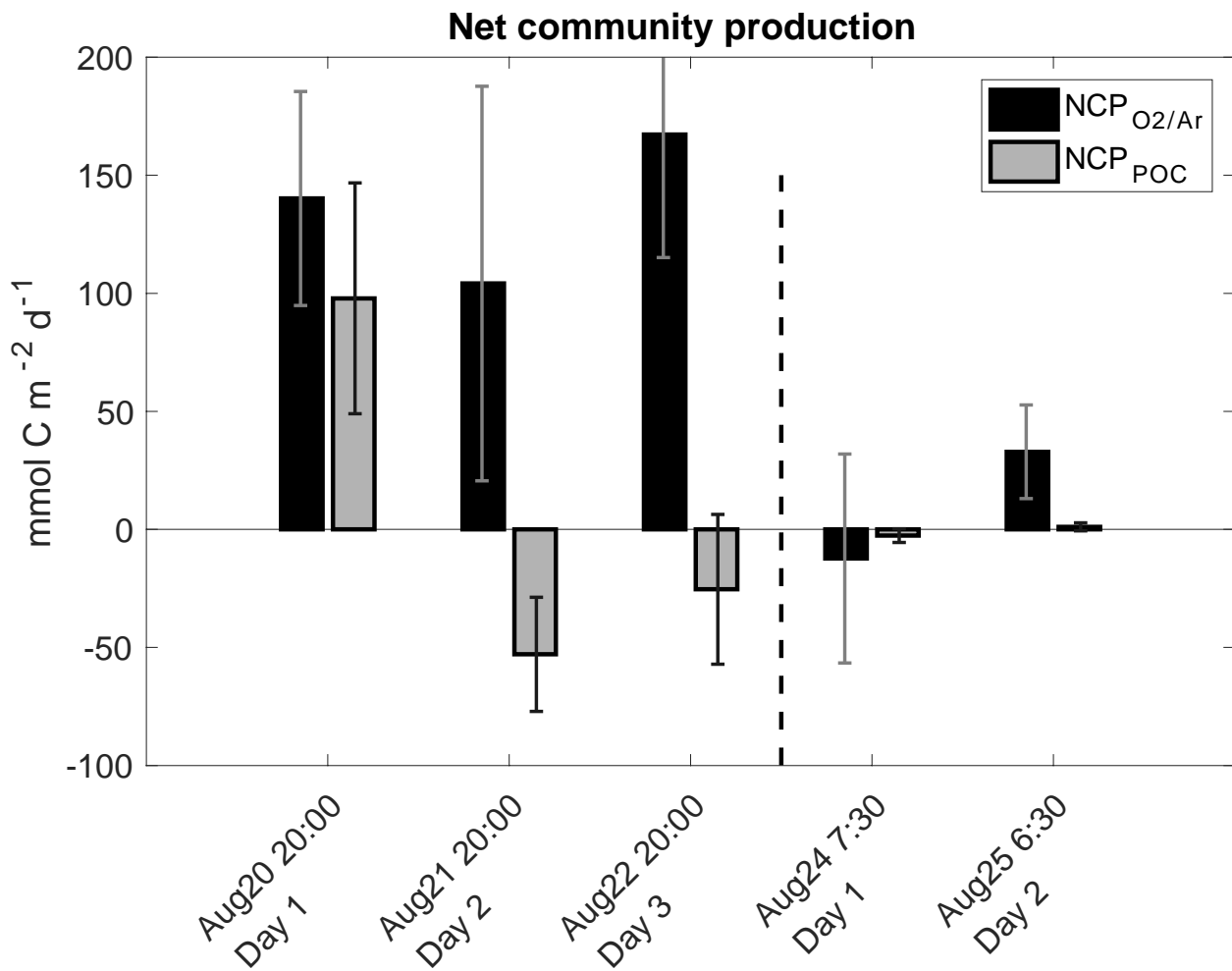
1364

1365

1366 **Figure 4**: Daily net community production (NCP) during successive days of the two drifter

1367 deployments derived from diurnal variations of biological oxygen saturation ($\Delta O_2/Ar$) and

1368 particulate organic carbon (POC) concentration. Each set of bars is for one 24-hour period, with

1369 approximate starting times on the x-axis. Note that the negative $NCP_{O2/Ar}$ value for the first day

1370 of drifter period 2 was computed by integrating $NCP_{O2/Ar}$ values over eight consecutive three-

1371 hour increments (refer to Table 2).
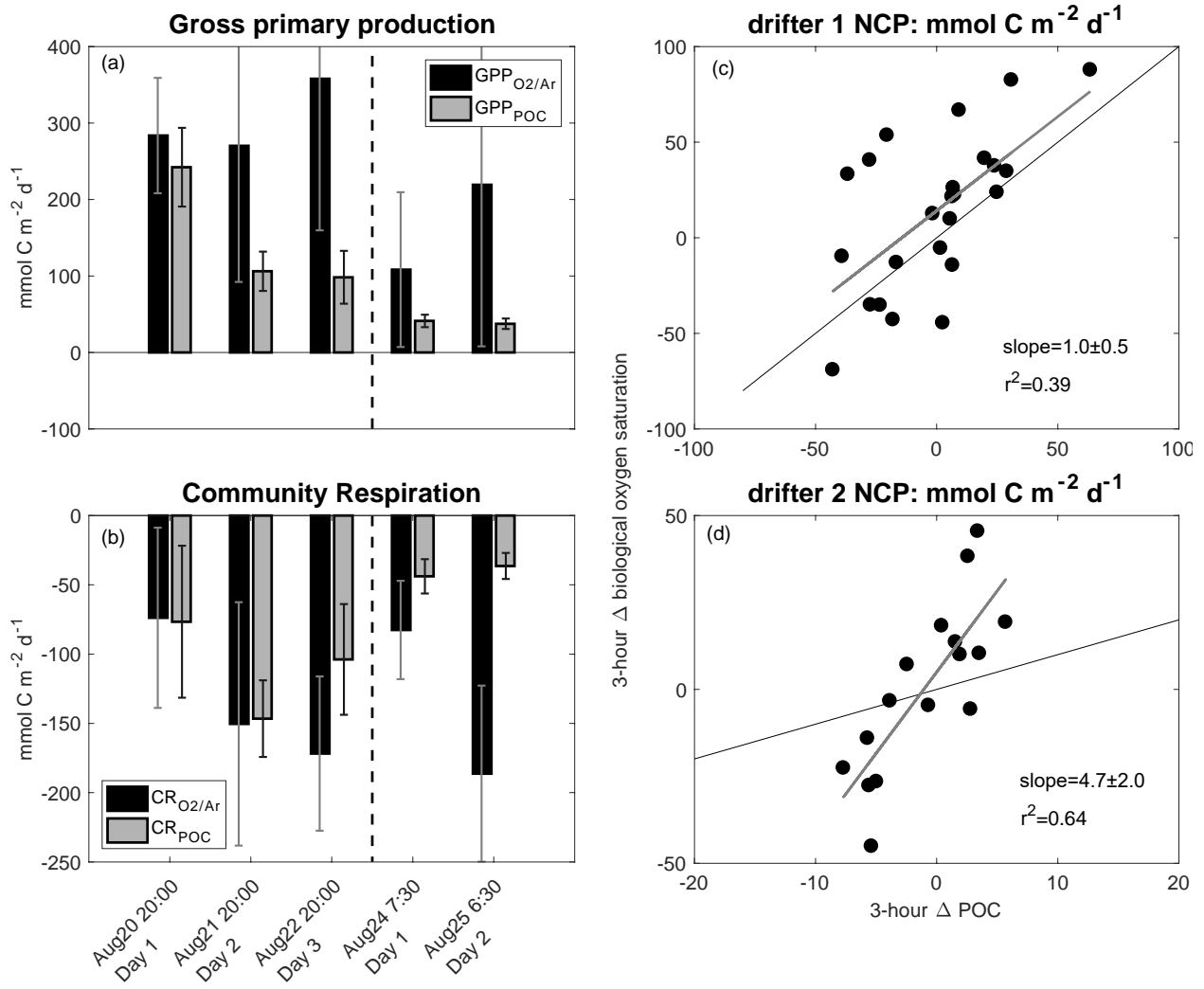
Figure 5: The left panels show comparisons between $\Delta O_2/Ar$-derived and POC-derived (a) GPP and (b) CR over the five days of both drifter deployments. The right panels show $\Delta O_2/Ar$-derived NCP (NCP$_{O2/Ar}$) as a function of POC-derived NCP (NCP$_{POC}$) over three-hour increments during (c) drifter period 1 and (d) drifter period 2. The vertical dashed lines in (a) and (b) indicate the break between drifter periods 1 and 2. Thin black lines in (c) and (d) represent the 1:1 line, while thicker grey lines are the best-fit from linear regressions and correspond to the indicated slope and r$_2$ values.